



This is a repository copy of *Empirical isochrones and relative ages for young stars, and the radiative-convective gap*.

White Rose Research Online URL for this paper:
<http://eprints.whiterose.ac.uk/138906/>

Version: Published Version

Article:

Mayne, N.J., Naylor, T., Littlefair, S.P. orcid.org/0000-0001-7221-855X et al. (2 more authors) (2007) Empirical isochrones and relative ages for young stars, and the radiative-convective gap. *Monthly Notices of the Royal Astronomical Society*, 375 (4). pp. 1220-1240. ISSN 0035-8711

<https://doi.org/10.1111/j.1365-2966.2006.11347.x>

This article has been accepted for publication in *Monthly Notices of the Royal Astronomical Society* ©: 2007 The Authors. Published by Oxford University Press on behalf of the Royal Astronomical Society. All rights reserved.

Reuse

Items deposited in White Rose Research Online are protected by copyright, with all rights reserved unless indicated otherwise. They may be downloaded and/or printed for private study, or other acts as permitted by national copyright laws. The publisher or other rights holders may allow further reproduction and re-use of the full text version. This is indicated by the licence information on the White Rose Research Online record for the item.

Takedown

If you consider content in White Rose Research Online to be in breach of UK law, please notify us by emailing eprints@whiterose.ac.uk including the URL of the record and the reason for the withdrawal request.



eprints@whiterose.ac.uk
<https://eprints.whiterose.ac.uk/>

Empirical isochrones and relative ages for young stars, and the radiative–convective gap

N. J. Mayne,^{1*} Tim Naylor,¹ S. P. Littlefair,² Eric S. Saunders¹ and R. D. Jeffries³

¹*School of Physics, University of Exeter, Stocker Road, Exeter EX4 4QL*

²*Department of Physics and Astronomy, University of Sheffield*

³*Astrophysics Group, School of Physical and Geographical Sciences, Keele University, Keele, Staffordshire ST5 5BG*

Accepted 2006 November 28. Received 2006 November 28; in original form 2006 September 5

ABSTRACT

We have selected pre-main-sequence (PMS) stars in 12 groups of notional ages ranging from 1 to 35 Myr, using heterogeneous membership criteria. Using these members we have constructed empirical isochrones in V , $V - I$ colour–magnitude diagrams. This allows us to identify clearly the gap between the radiative main sequence and the convective PMS (the R–C gap). We follow the evolution of this gap with age and show that it can be a useful age indicator for groups less than $\simeq 15$ Myr old. We also observe a reduction in absolute spreads about the sequences with age. Finally, the empirical isochrones allow us to place the groups in order of age, independently of theory. The youngest groups can be collated into three sets of similar ages. The youngest set is the ONC, NGC 6530 and IC 5146 (nominally 1 Myr); next Cep OB3b, NGC 2362, λ Ori and NGC 2264 (nominally 3 Myr); and finally σ Ori and IC 348 (nominally 4–5 Myr). This suggests Cep OB3b is younger than previously thought, and IC 348 older. For IC 348 the stellar rotation rate distribution and fraction of stars with discs imply a younger age than we derive. We suggest this is because of the absence of O-stars in this cluster, whose winds and/or ionizing radiation may be an important factor in the removal of discs in other clusters.

Key words: techniques: photometric – catalogues – stars: evolution – stars: formation – Hertzsprung–Russell (HR) diagram – stars: pre-main-sequence.

1 INTRODUCTION

Most ages for stellar groups, subgroups, clusters or associations are derived from fitting observations to theoretical isochrones. It is well known that these models often deviate systematically from the data. For instance if the isochrone fits part of a sequence it may systematically deviate from the observed sequence in other sections (e.g. Bonatto, Bica & Girardi 2004; Pinsonneault et al. 2004). In addition if a sequence of stars is fitted to an isochrone in one colour, derived parameters such as the age may be different from those derived in another colour (e.g. Naylor et al. 2002). In this paper we create empirical isochrones. These have the advantage of necessarily fitting the entire data sequence, allowing us to create a relative age ladder. We can then derive ages for fields where different regions of a sequence are available by selecting appropriate fiducial sequences covering the required colour range. The obvious disadvantage of our empirical isochrones is that they are unable to provide absolute age information. Although this is the first attempt to create such a ladder, carried out with data that uses slightly different photometric

systems and heterogeneous selection criteria, the method is clearly effective.

As we have used a range of ages to create the empirical isochrones we are able to examine how these isochrones change with age. In many fields this reveals a clear gap between the convective lower mass pre-main-sequence (PMS) and the radiative stars close to or on the main sequence (MS). We refer to this feature as the radiative–convective gap (R–C gap).

For this study we have used the optical bands V and I . This enables us to minimize the effect of accretion, disc presence and chromospheric activity on our empirical isochrones. Accretion will generally affect the flux shortward of the B band (Gullbring et al. 1998) with disc emission important at longer wavelengths, first becoming significant in the H and K bands (Hartmann 1998). Lastly, Stauffer et al. (2003) have shown that magnetically generated chromospheric activity in young stars primarily causes perturbations and scatter in the $B - V$ and $U - B$ colours, whereas the V , $V - I$ colour–magnitude diagram (CMD) is unaffected.

Our paper is laid out as follows. The data collection and reduction are detailed in Section 2. To create the empirical isochrones we select members in each field using a variety of criteria (see Appendix A and Section 3.3) and fit a curve through these in a V ,

*E-mail: nathan@astro.ex.ac.uk

$V - I$ CMD (see Section 3.2). We then apply a distance modulus and correct for extinction (see Section 4). The reader may wish to move straight to Section 5. Here we present the data corrected for distance and extinction, allowing comparisons to be made with theory and also between sequences from clusters, groups or associations of different ages. Finally, we combine the sequences to form a fiducial relative age ladder (see Section 6), which we then use to find new age estimates for six fields (see Section 7). In Section 9 we summarize our conclusions. Appendix A contains a discussion of the literature membership data, while in Appendix B we discuss the distances and extinctions from the literature that we have used.

2 DATA COLLECTION

The data set used in this paper is from both new observations and literature sources.

2.1 New observations

The images for the majority of this data set were obtained in *BVI* with the 2.5-m Isaac Newton Telescope (INT), situated on La Palma, equipped with the four EEV CCD Wide Field Camera (WFC). The filters used were Sloan i' and Harris V and B . The data sets used were collected on the nights of 2004 September 27 and October 5, when the range of seeing was 1–2 and 1–1.5 arcsec on each night, respectively. Both nights were photometric. The observational details are given in Table 1. Standards from Landolt (1992) were observed on these photometric nights, tying our calibration to B , V and I_c Landolt standards.

2.2 Data reduction

The images were debiased, and then flat fielded using median stacks of many sky flat frames. The i -band images were then defringed using a library fringe frame. Known bad pixels were flagged. The data, including the standards, were then reduced following the optimal extraction algorithm detailed in Naylor (1998) and Naylor

et al. (2002). We used the Two Micron All-Sky Survey (2MASS) to provide an astrometric solution for each field accurate to $\simeq 0.1$ arcsec. The reduction process provided catalogues of photometry with flags and uncertainties. The flags are explained in Burningham et al. (2003), excepting the flag T. These are objects where the profile correction (see Naylor et al. 2002) fails due to a paucity of stars in the field. Therefore aperture photometry is performed using an aperture of the same radius as that to which the optimally extracted fluxes are corrected. Since aperture photometry is noisier than optimal photometry, we only carry out this procedure for the brighter stars, hence the fluxes for fainter stars in the same image will be optimally extracted, and flagged as having poor profile corrections (H).

Photometric calibration coefficients were calculated from the standard star observations using a similar procedure to that detailed in Pozzo et al. (2003). For each colour or magnitude we allow the following free parameters: one extinction coefficient per night; one colour term for each CCD; one zero-point for each night, with offsets with respect to this (which do not change from night to night) for three of the four CCDs. The standards used had colour ranges of $-0.30 < V - I < 2.87$ and $-0.30 < V - I < 2.85$, with air-mass ranges of 1.13–1.32 and 1.14–1.22, on 2004 September 27 and October 5, respectively.

We estimate the combined uncertainty in profile correction and transformation to the Landolt system by adding a magnitude independent uncertainty. Adding 0.02 mag in each band gave a reduced χ^2 of approximately one in V and $B - V$. The value of reduced χ^2 was somewhat higher in $V - I$ (1.4), which we suspect is due to the poor match between our i filter and those used by Landolt.

In the cases where multiple fields were observed (NGC 2264, σ Ori and h and χ Per) the catalogues were combined using the method described in Naylor et al. (2002). Overlapping regions were used to normalize the photometry to provide a combined catalogue. As detailed in Naylor et al. (2002) the rms of the overlap region is a good measure of the accuracy of the profile correction. This suggests a magnitude independent uncertainty of approximately 0.01 mag which should be added to all bands when comparing objects well separated on the CCDs. Using the overlap region suggest an accuracy of 1 per cent in both V and $B - V$ and around 2 per cent in $V - I$. We believe the higher uncertainty in $V - I$ is caused by a lack of redder standards across all the CCDs. This uncertainty is not included in the catalogues. For all subsequent analysis the combined catalogues have been used.

All of the new catalogues used for this paper are freely available from the cluster collaboration home page,¹ and the CDS archive (sample can be seen as Table 4). For membership selection and CMD plots we exclude stars with uncertainties greater than 0.1 mag in colour or magnitude. The machine readable catalogues retain all the data.

To aid navigation through this paper an index to the catalogues is included as Table 2. Full catalogues are presented for each field with new photometry in addition to catalogues of stars which fulfil given membership criteria.

2.3 Literature data

Literature observations were taken in all cases (except where stated) in the Johnson–Cousins photometric system using I_c (Cousins I). This raises the question of what effect the use of two different I filters has on our results. The difference is illustrated in Fig. 1. The

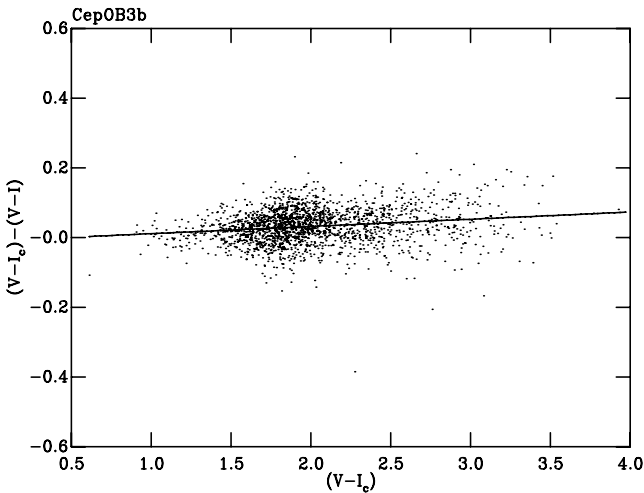
Table 1. Exposure times for each field.

Field	Filter	Exposure time (s) ($\times 1$ unless stated)
h Per	I	3 and 30
	V	1, 10 and 100
	B	2 and 20
χ Per	I	3 and 30
	V	1, 10 and 100
	B	2 and 20
NGC 7160	I	3 and 30
	V	1, 10 and 100
	B	2 and 20
NGC 2264 (4 fields)	I	2 and 20
	V	2 and 20
	B	4 and 40
IC 348	I	2 and 20
	V	2 and 20
	B	4 and 40
Cep OB3b	I	5($\times 2$), 30($\times 2$) and 300($\times 2$)
	V	5, 30 and 350($\times 4$)
σ Ori (Fields 1,2 and 4)	I	2 and 20
	V	2, 10, 100 and 350($\times 4$)
σ Ori (Field 3)	I	2 and 20
	V	2, 10, 100 and 350
	B	4

¹ <http://www.astro.ex.ac.uk/people/timn/Catalogues/description.html>

Table 2. The catalogues presented in this paper.

Region	Table number	Data	Source (as Table 3)
NGC 2547	4	Members	1 (X-ray)
	5	Members	2 (spectroscopy)
NGC 7160	6	Full catalogue	
	7	Members	3 (extinction)
NGC 2264	8	Full catalogue	
	9	Members	6 (periodic variables)
Cep OB3b	10	Members	4 (X-ray)
	11	Members	5 (H α)
	12	Members	26 (proper motion)
	13	Full catalogue	
	14	Members	7 (X-ray)
σ Ori	15	Members	8 (spectroscopy)
	16	Members	18 (periodic variables)
	17	Members	19 (H α)
	18	Members	25 (X-ray)
σ Ori	19	Full catalogue	
	20	Members	11 (X-ray)
IC 348	21	Members	12 (spectroscopy)
	22	Full catalogue	
IC 348	23	Members	10 (periodic variables)
	24	Members	16 (X-ray)
	25	Members	15 (X-ray)
	26	Members	9 (spectroscopy)
	27	Members	17 (H α)
h and χ Per	28	Full catalogue (combined)	
	29	Positionally isolated	

**Figure 1.** The difference in $V - I$ for Cep OB3b between data taken in the system used here and using Cousins I_c filter. The line is the best fit through the data.

data for Sloan i , for stars in Cep OB3b is from this work and the data for Cousins I_c , for the same stars is taken from Pozzo et al. (2003). The symbol I from hereon will be used to represent data taken using a Sloan i filter tied to the Landolt standards, with I_c being data taken in Cousins I_c tied to Landolt standards. The difference $(V - I_c) - (V - I)$ is plotted as a function of $(V - I_c)$ in Fig. 1. The data can be represented by the following linear fit: $(V - I) = 0.979(V - I_c) + 0.009$. This result shows that two stars with an apparent $V - I$ of 3 mag, one cool and unreddened, that is, a typical Landolt standard, and another hotter and more heavily reddened, need not have the

same $V - I_c$. As demonstrated by the extreme example of CepOB3b ($A_V \simeq 3$ mag), even at a $V - I = 3$ the shift is <0.1 mag; though note that the reddest standard in our $V - I$ calibration is 2.87. This means over the colour range covered within this paper the effect is negligible.

3 SEQUENCE ISOLATION AND FITTING

For each field of view (FOV) the CMD includes a high proportion of background and foreground objects, therefore we faced the common problem of identifying members. For most fields we used literature sources for members. We discuss these fields in Sections 3.1 and 3.2. For h and χ Per no membership data were available for the group, or none at faint enough magnitudes. Here we can increase our confidence in selecting the correct sequence by selecting a limited area of the sky. This method will clearly include a higher proportion of non-members. The field treated in this way is discussed in Section 3.3.

3.1 Sequences with memberships

In Appendix A we collect literature membership data for each field, a summary of which is presented in Table 3. We use a wide range of membership criteria, each of which will have an implicit bias. As we are interested in the form of the sequences in CMD space it is important to be aware of and limit any bias incurred with respect to the CMD space. X-ray selection will be biased to weak lined T Tauri stars (WTTS) and binary systems (Preibisch & Feigelson 2005). Variability exhibits a bias towards accreting objects, though periodic variability may exclude many classical T Tauri stars (CTTS) objects when observed over a long baseline. However, periodic variability deduced from a short baseline does not carry this bias (Littlefair

Table 3. Table of literature sources and astrometric matching criteria.

Group	Data type	Source	Matching radius	Offsets RA, Dec. (arcsec)
NGC 2547	X-ray (<i>ROSAT</i>)	1	From 1	0 0
	Spectroscopy	2	1 arcsec	0 0
NGC 7160	Extinction	3	1 arcsec	0 0
NGC 2264	X-ray (<i>ROSAT</i>)	4	6 arcsec	0 0
	H α	5	1	0 0
Cep OB3b	Periodic variables	6	1 arcsec	0 0
	X-ray (<i>ROSAT</i>)	7	From 7 otherwise 14 arcsec	0 0 (both)
	X-ray (<i>Chandra</i> ACIS)	25	1	0 0
	Spectroscopy	8	1 arcsec (both)	0 0 (both)
	H α	19	1 arcsec	0 0
σ Ori	Periodic variables	18	1 arcsec	0 0
	X-ray (XMM-NEWTON)	11	6 arcsec	0 0
ONC	Spectroscopy	12	1 arcsec (both)	0 0 (both)
	Periodic variables	13	1 arcsec	+1.5 –0.25 and 0 0
IC 348	X-ray (<i>Chandra</i>)	14	2 arcsec	0 0
	Periodic variables	10	1 arcsec	–0.1 –0.5
	X-ray (<i>Chandra</i> ACIS)	16	1 arcsec	–0.5 0
	X-ray (<i>ROSAT</i>)	15	14 arcsec	0 0
	Spectroscopy	9	1 arcsec (both)	0 0 and +0.2 –0.5
NGC 2362	H α	17	1 arcsec	+0.2 –0.5
	H α (Li)	20	Members from 20	
λ Ori	Spectroscopy (Li)	21	Members from 21	
IC 5146	H α	22	1	0 0
NGC 6530	H α	23	Members from 23	
	X-ray (<i>Chandra</i> ACIS)	24	Members from 24	

(1) Jeffries & Tolley (1998), (2) Jeffries & Oliveira (2005), (3) Sicilia-Aguilar et al. (2005), (4) Flaccomio et al. (1999), (5) Dahm & Simon (2005), (6) Lamm et al. (2004), (7) Second *ROSAT* PSPC catalogue and Naylor & Fabian (1999), (8) Pozzo et al. (2003) and Ogura et al. (2002), (9) Luhman et al. (2003) and Herbig (1998), (10) Cohen et al. (2004) and Littlefair et al. (2005), (11) Sanz-Forcada et al. (2004), (12) Burningham et al. (2005b) and Kenyon et al. (2005), (13) Herbst et al. (2002), (14) Flaccomio et al. (2003), (15) Second *ROSAT* PSPC catalogue, (16) Preibisch & Zinnecker (2002), (17) Herbig (1998), (18) Littlefair et al. (in preparation), (19) Ogura et al. (2002), (20) Dahm (2005), (21) Dolan & Mathieu (2001), (22) Herbig & Dahm (2002), (23) Sung et al. (2000), (24) Prisinzano et al. (2005), (25) Getman et al. (2006) and (26) Mendoza & Gomez (1980).

et al. 2005). The final frequently used data source was H α , which is generally biased towards CTTS.

There is also a more subtle form of bias due to pre-selection. Because in many cases surveying all objects in a field is not possible, an observer will necessarily select a subset of objects. Often this initial selection is based on the positions of objects in CMD space thus introducing a bias in CMD space. This is particularly applicable to spectroscopic data. Where this form of sample selection has occurred the selection criteria are stated clearly in Appendix A.

Samples derived from non-spectroscopic methods of membership selection have a higher probability of containing contamination from background (BG) or foreground (FG) objects. This leads to the need for colour–magnitude selections to remove data points which lie far from the group sequence. Where we have done this the number of discarded objects is small relative to the total number of objects and has little effect on the final sequence (see Section 3.2). In each section where such a selection was used, it is shown in the CMD and its effect on the result is discussed.

3.2 Fitting procedure

To explain the stages involved in producing the empirical isochrones we use an example cluster, NGC 2264. This cluster is a good illustration as it has a large number of members from various sources.

3.2.1 NGC 2264: an example

Once the sequence was finalized to stars having properties indicative of cluster membership (see Appendix A1) we fitted the median filtered sequence with a smooth curve. The median filter was used for two reasons. The median is necessarily tied to the values of real stars. In addition the median allows the effect of stars lying far from the sequence to be limited, as not all of our memberships are certain, for instance the X-ray sources in this group. The median of any sequence was calculated by binning the stars in V -band intervals and assigning the median $V - I$ and V values to the median star for that bin. The bin sizes were tailored to each field, and we enforced a minimum number of stars in each bin. A cubic spline was fitted through the resulting list of median stars, over the colour range of the stars selected, with the gradients at the ends tied to a quadratic. The resulting fit for NGC 2264 is shown in Fig. 2.

To remove BG and FG objects and spurious matches which lie below the PMS a colour–magnitude selection was applied before fitting. We removed objects lying below the dotted line in Fig. 3. We were concerned by the effect of this colour–magnitude selection on the spline functions, so we examined fits using data with and without a selection. The effect of removing the colour–magnitude selection for NGC 2264 is shown in Fig. 3. It has little effect on the resulting spline.

The resulting fit is clearly an average through the spread in the CMD (sometimes referred to as an age spread, see Burningham et al.

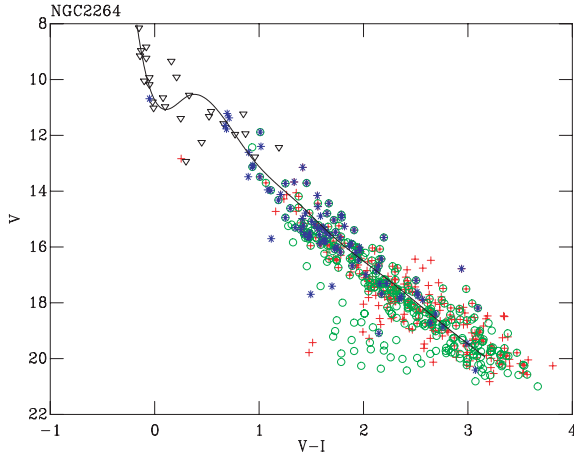


Figure 2. Stars selected as members of NGC 2264. Circles are the periodic variables from Lamm et al. (2004), asterisks are X-ray sources from Flaccomio et al. (1999), crosses are H α sources from Dahm & Simon (2005) and triangles are proper motion members from Mendoza & Gomez (1980). The spline fit to the sequence after a colour–magnitude selection is shown.

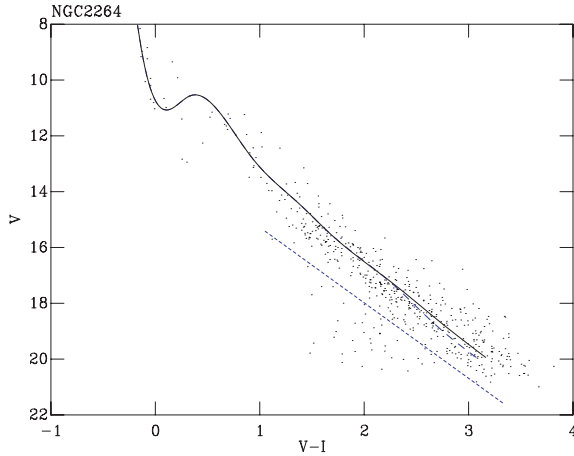


Figure 3. The effect of choosing a wider colour–magnitude selection in NGC 2264. The effect is limited by the large number of sources within the sequence. The solid curve is the result using no selection, with the dotted line being the colour–magnitude selection and the dashed line the spline fit after the colour–magnitude selection is enforced, that is, only stars above the line were used to produce the spline curve.

2005a, and references therein). Part of this spread will be due to unresolved binaries which lie above the single star sequence, lifting the spline above the single star sequence. Thus our splines do not necessarily follow the single-star sequence, although the displacement due to binary should be the same for all fields. Furthermore the scale of this effect is small, as can be seen in the CMDs where there is a clear separation between the binary and single star sequence, for example, NGC 2547 (Fig. 4).

Sometimes the spline fit does not precisely follow the sequence the eye picks out, for example, $0.5 < V - I < 1$ for NGC 2264. Whether the spline or the eye is correct turns out to be immaterial. The deviations are never large enough to affect our conclusions.

3.2.2 NGC 2547

The observations of NGC 2547 were taken from Naylor et al. (2002), using Cousins I_c . The photometry was calibrated with coefficients

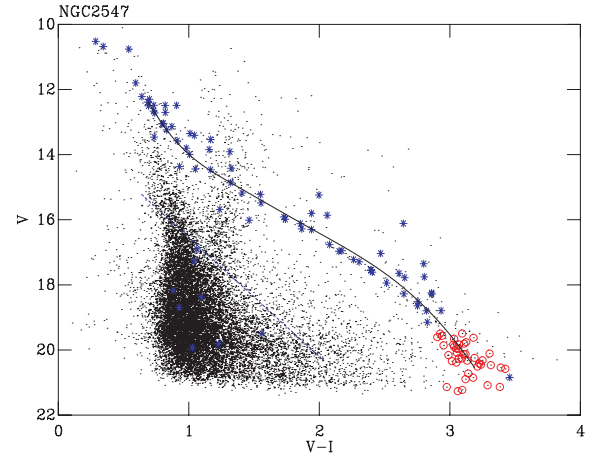


Figure 4. The full catalogue for the NGC 2547 field (dots). Asterisks are the X-ray sources from Jeffries & Tolley (1998), circles are spectroscopic members from Jeffries & Oliveira (2005). The X-ray sources, some of which clearly lie in the BG MS contamination were removed using a colour–magnitude cut prior to fitting, shown here as the dotted blue line.

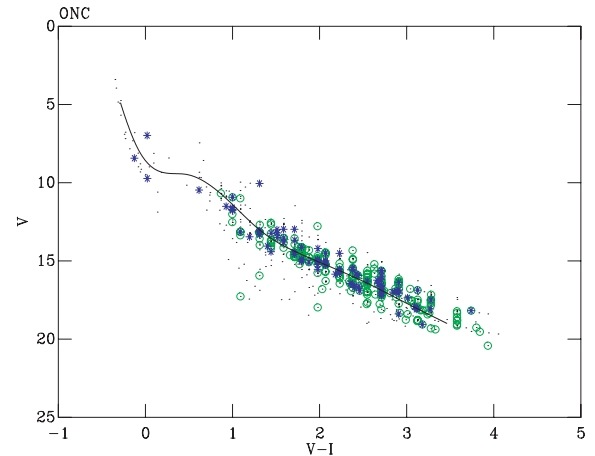


Figure 5. The ONC photometry from Hillenbrand (1997) (dots). Circles are objects which are periodic variables from Herbst et al. (2002). The asterisks are X-ray sources from Flaccomio et al. (2003). The best-fitting spline through all data points is also shown.

detailed in Naylor et al. (2002) with the reddest standard having a $V - I$ of 2.7. The resulting fit, after sequence selection is shown in Fig. 4. A colour–magnitude selection was used to clip out probable non-members. Only eight objects were removed, all lying far from the sequence and within the contamination. The fitted line lies slightly above the single star sequence, an effect due to binary stars.

3.2.3 ONC

The photometry (using I_c) and membership probabilities for this region come from Hillenbrand (1997). For the ONC the extinctions are calculated individually for each star, therefore the order in which the fitting and conversion to absolute colours and magnitudes is carried out is crucial. Where average extinctions have been used the entire space is simply translated and the fitted spline curve will not change shape. If however individual extinctions are used shifts may therefore be different for each object, changing the shape of the sequence. Consequently, for the ONC the extinctions must be

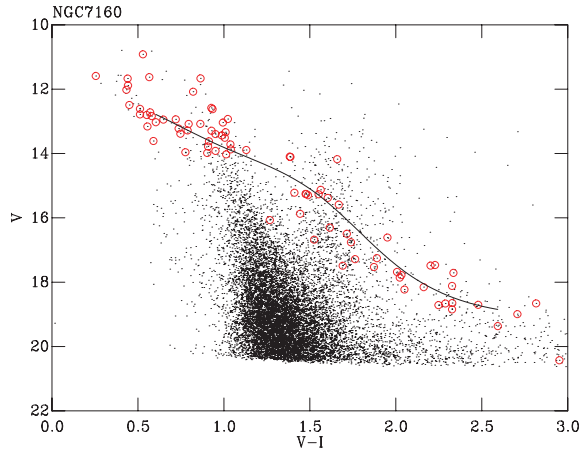


Figure 6. The full catalogue for the NGC 7160 field (dots). Circles are members from Sicilia-Aguilar et al. (2004) and Sicilia-Aguilar et al. (2005).

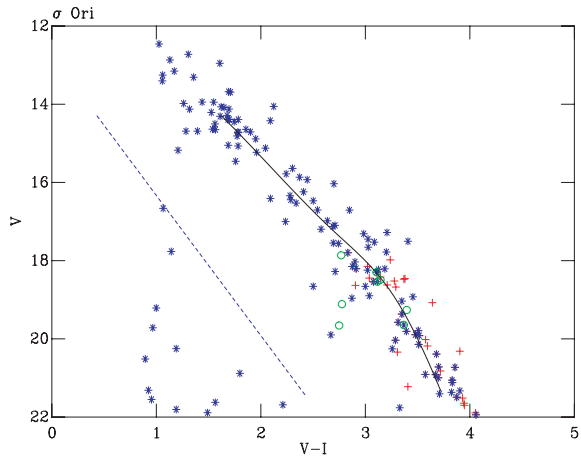


Figure 7. Stars selected as members in σ Ori. Circles are Burningham et al. (2005b) members. Asterisks are X-ray sources from Sanz-Forcada, Franciosi & Pallavicini (2004). Crosses are members from Kenyon et al. (2005). The fitted spline curve is shown. The colour–magnitude selection is shown as the dotted line.

applied before the fitting procedure. This is also the case for the later fields of IC 348 and IC 5146. The resulting sequence (extinction corrected) with additional membership information fitted is shown as Fig. 5. All the stars shown were fitted to yield the spline curve shown. No colour–magnitude selection was utilized here as nearly all the stars within 15 arcmin of the centre are members of the ONC. This is because the background stars are largely obscured by the dense cloud behind the cluster.

3.2.4 NGC 7160

The sequence and fit is displayed in Fig. 6. The members, although sparse, represent a relatively unbiased sample in CMD space due to the ‘wide’ criteria applied to assign memberships (see Section A4).

3.2.5 σ Ori

For σ Ori a colour–magnitude selection was used to clip out the X-ray sources lying within the contamination. The resulting line fit is displayed in Fig. 7. The applied colour–magnitude selection

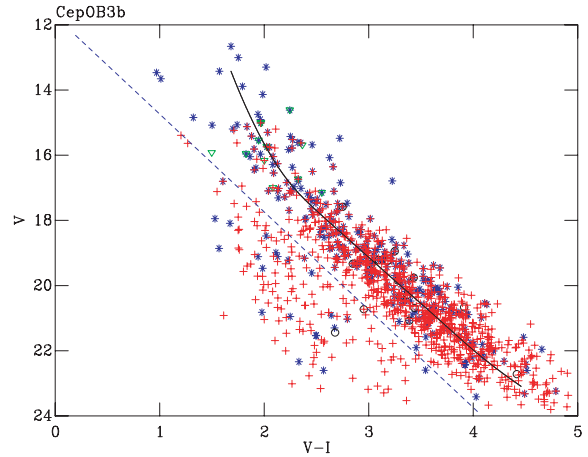


Figure 8. Stars selected as members in Cep OB3b. Asterisks are X-ray sources from Naylor & Fabian (1999), Getman et al. (2006) and the second PSpC catalogue. Triangles are members from Pozzo et al. (2003). Circles are $H\alpha$ sources from Ogura, Sugitani & Pickles (2002). Crosses are the periodic variables from Littlefair et al. (in preparation). The fitted spline curve is shown.

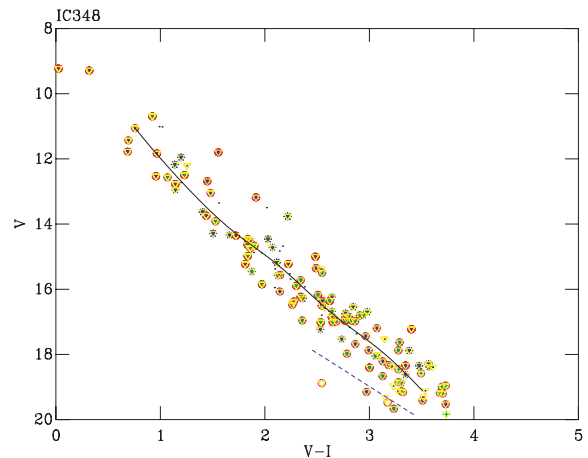


Figure 9. Stars selected as members in IC 348. The asterisks are X-ray sources from Preibisch & Zinnecker (2002) and the Second *ROSAT* PSpC catalogue. Circles are the periodic variables from Cohen, Herbst & Williams (2004) and Littlefair et al. (2005). Crosses are $H\alpha$ sources from Herbig (1998). Triangles are spectroscopic members with extinctions from Luhman et al. (2003) and Herbig (1998). Individual extinctions from Luhman et al. (2003) and Herbig (1998) have been applied before fitting.

removed five objects all far from the sequence and within the contamination.

3.2.6 Cep OB3b

The selected members and fit for Cep OB3b are shown as Fig. 8. A colour–magnitude selection has again been applied, although as in Section 3.2, since most objects lie in the sequence the effect on the fit is negligible.

3.2.7 IC 348

For IC 348 individual extinctions were available for all but 21 of the members. Therefore only those members with extinctions have been

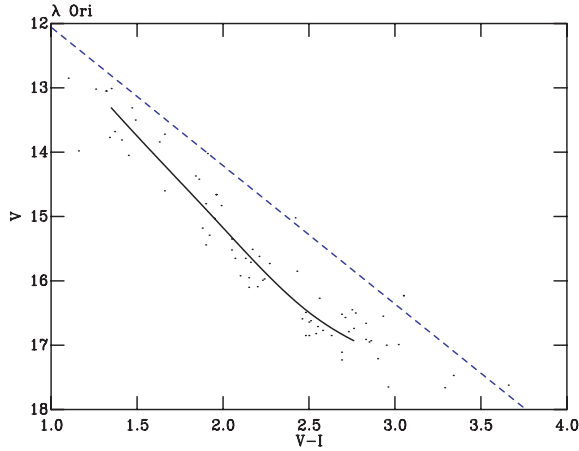


Figure 10. Stars selected as members in λ Ori. The dots are Li members from Dolan & Mathieu (2001).

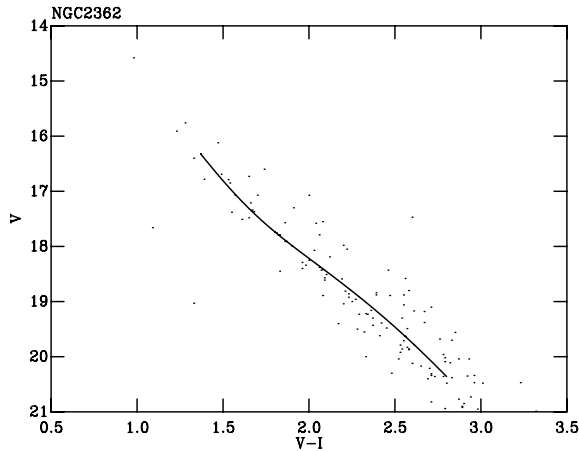


Figure 11. Stars selected as members in NGC 2362. The dots are H α and spectroscopically confirmed PMS members from Dahm (2005).

used. A colour–magnitude selection has been applied removing five stars below the sequence. The individual dereddenings were applied prior to fitting. The dereddened sequence with the fitted curve can be seen as Fig. 9.

3.2.8 λ Ori, NGC 2362, IC 5146 and NGC 6530

The data for λ Ori are from Dolan & Mathieu (2001) taken in the Johnson–Kron–Cousins system and calibrated to Landolt standards, a colour–magnitude selection has been applied removing three stars lying well above the sequence. The data for NGC 2362 are from Dahm (2005), taken with an I_c filter and tied to Landolt standards. The Cousins photometry for IC 5146 comes from Herbig & Dahm (2002), here only the stars shown as asterisks in Fig. 12 were fitted. This contains photometry from two areas approximately 10 arcmin apart. The photometry for NGC 6530 is from Prisinzano et al. (2005). The members and spline fits for these fields can be seen as Figs 10–13.

3.3 Isolating the sequence for h and χ Per

In this field there was no membership data of the form used above, so colour–magnitude selections were employed. In addition as the

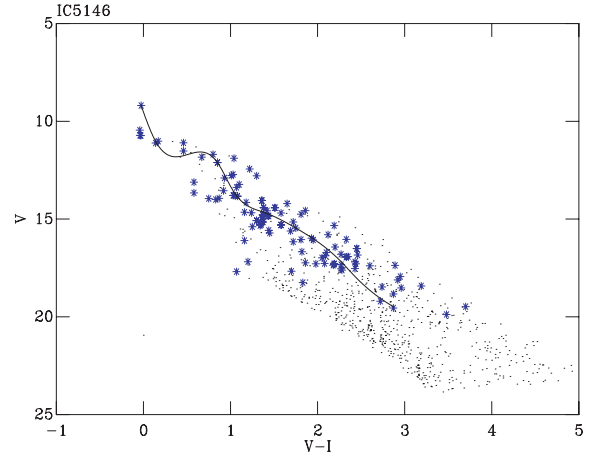


Figure 12. Stars selected as members in IC 5146. Dots are likely PMS members from Herbig & Dahm (2002). Asterisks are H α members from Herbig & Dahm (2002) with known spectral types excluding stars lying below the Pleiades MS. Only the asterisks were fitted.

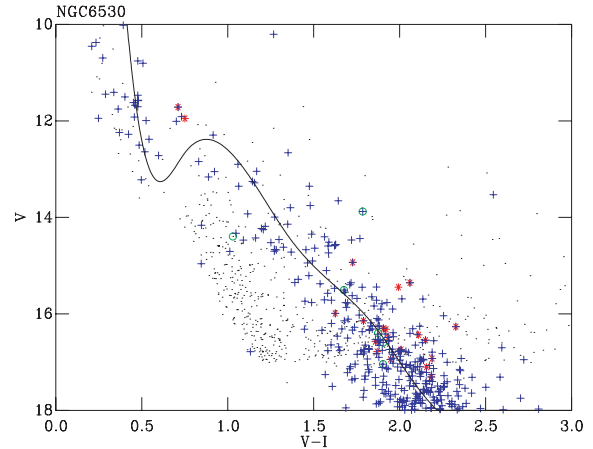


Figure 13. The photometry of NGC 6530 from Prisinzano et al. (2005) (dots). Crosses are X-ray sources from Prisinzano et al. (2005). Circles are weak H α stars from Sung et al. (2000). Asterisks are strong H α stars from Sung et al. (2000).

group in question is clustered in the FOV it was possible to remove a proportion of FG and BG objects by selection of a limited area of the FOV. We however needed a guiding mechanism to allow us to pick the approximate central coordinates and a subsequent area to isolate. The following procedure was undertaken to isolate the cluster in celestial coordinates.

(1) *Lead stars:* We show our CMD for the full h and χ Per catalogue in Fig. 14. The sequence is clearly visible and the brighter stars clearly lie blueward of the contamination. Therefore the positions of these stars on the sky were plotted, allowing us to trace the outline of the clusters. This can be seen in Fig. 15.

Three other sets of lead star candidates were explored. Uribe et al. (2002); proper motion members or photometric members from Slesnick, Hillenbrand & Massey (2002) and Muminov (1996). The coordinates from each set were carried forward through the following steps. However, the central coordinates for all cases were very similar.

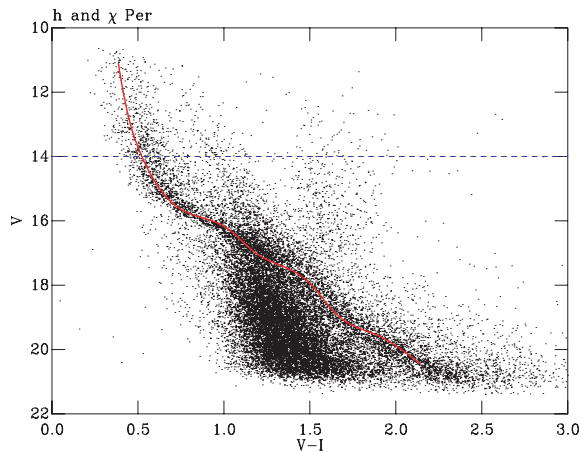


Figure 14. The full catalogue for the h and χ Per field (dots). The dotted line shows a colour–magnitude selection of $V < 14$, showing the sequence clear of the contamination. The solid line is the best-fitting spline to the selected sequence corrected to the mean extinction for the two clusters.

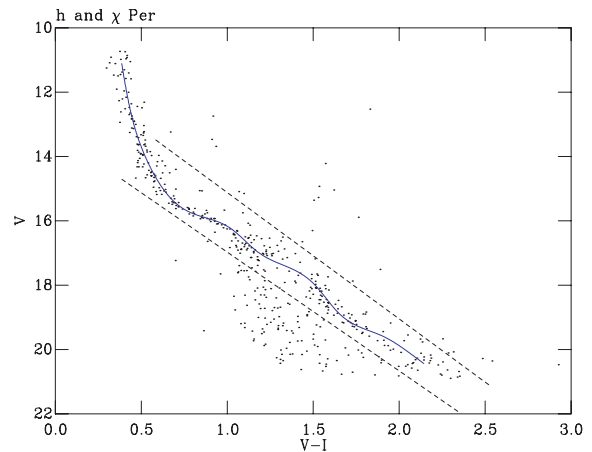


Figure 16. Stars within 2 arcmin radius of the centres of h and χ Per. Stars in the h Per region have been shifted in extinction to match those χ Per. The dotted lines are the colour–magnitude cuts used, and the solid curve the best-fitting spline.

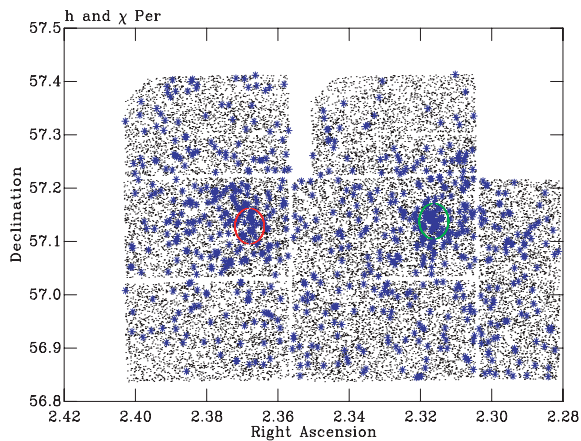


Figure 15. The positions of stars in the h and χ Per catalogue. Asterisks are stars with $V < 14$, and the large circles show the regions we selected.

(2) *Positional selection:* A circular positional selection was applied to the full catalogue around the central coordinates, with an inclusion radius varying from 5 arcmin down to 1 arcmin in increments of 1 arcmin. The CMDs for each were examined and a ‘by eye’ selection made for the CMD yielding the clearest sequence, optimizing the member to field-object ratio. The best results were obtained with a radius of 2 arcmin. The final central coordinates for each cluster are: $\alpha = 2^\circ 22' 5''.028 = +57^\circ 7' 43''.44$ (χ Per), $\alpha = 2^\circ 18' 58''.768 = +57^\circ 8' 16''.54$ (h Per), J2000.

Since the measured ages in virtually all the literature for h and χ Per are the same, it was possible to increase our confidence of selecting the correct sequence in CMD space by combining the CMDs from both clusters. To achieve this any differences in extinction and distance modulus must be accounted for. We derived extinctions and distance modulus shifts in the sense h Per minus χ Per using three methods.

(i) Matching the curve in the MS at $V = 16$ mag for both clusters by eye, we found $A_V = 0.08 \pm 0.05$, $d_m = 0.07 \pm 0.05$ mag.

(ii) Matching the centre of the UMS (upper main sequence) of χ Per to the centre of the more scattered UMS in h Per gave

a shift in $|d_m|$ of < 0.05 , with a shift in extinction of $A_V = 0.2 \pm 0.05$.

(iii) The Q-method (see Section 4.1) gave $A_V = 0.157 \pm 0.0212$.

We chose the Q-method value for the extinction and no shift in d_m . The scatter in the different derivations suggests an uncertainty of approximately ± 0.05 in extinction and distance modulus. This shift was applied to h Per, and the combined catalogue used from thereon (Table 28; see caption of Table B1, below). The final area selected can be seen overlaid on Fig. 15.

(3) *Colour–magnitude selection and fitting:* The final sequence was then fitted as described in Section 3.2. Cuts in colour–magnitude space were then used to clip out stars lying far from the sequence. The cuts were varied until a best fit of the spline curve to the sequence was achieved. The final sequence, cuts and spline curve are shown in Fig. 16. To further increase our confidence in selection of the correct sequence the best-fitting spline was shifted to the mean extinction for both clusters and overlaid on the CMD showing the full catalogue. The spline curve clearly follows the sequence one would select by eye from this CMD, see Fig. 14.

4 PARAMETERS

To compare the data for our sequences on a single CMD we required estimates for the extinction (A_V) and true distance modulus (d_m). To obtain a self-consistent set of empirical isochrones it is clearly better to use a single method to determine extinction. This was possible for a range of fields using the Q-method as detailed below. Where data for the Q-method were unavailable we have used values from the literature, given in Appendix B, below. A summary of the distance moduli and extinctions we used can be found in Table B2, with a summary of the results from the Q-method given in Table B3.

4.1 Q-method

Using *UBV* photometry from the literature we applied the Q-method of Johnson & Morgan (1953). This method uses the colour relationships of OB stars and is only valid over a small range of spectral types. Johnson & Morgan (1953) quote $(B - V)_0 = -0.009 + 0.337Q$ to be valid for $-0.80 < Q < -0.05$, converting to an

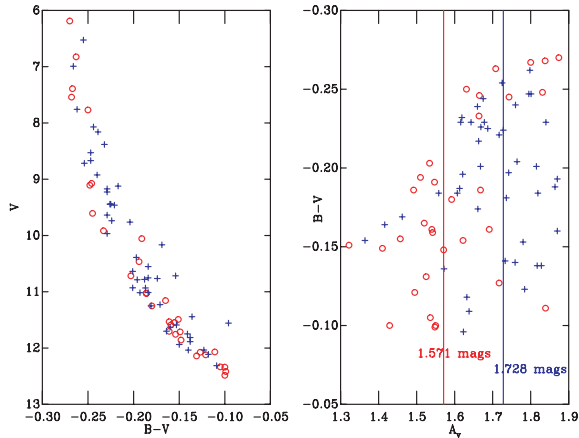


Figure 17. Left-hand panel: The sequences for h and χ Per O and B stars after the application of the Q-method. Right-hand panel: The extinction. The circles are χ Per and the crosses are h Per. The resulting median values of $A_V = 1.571$ and 1.728 for χ and h Per, respectively, are shown.

intrinsic colour range of $-0.28 < (B - V)_0 < -0.03$. This was used in conjunction with the initial parameter estimates to calculate an apparent colour range over which the method was applicable in each field. We then derived a mean extinction which we could in turn apply to our selection. The loop of applying a mean extinction, calculating Q from the stars within the colour range and calculating a new mean extinction was iterated until the number of stars used in successive iterations remained constant. The rms around the mean value divided by the square root of the number of points provides an uncertainty.

4.1.1 h and χ Per

Here UBV photometry was obtained from Slesnick et al. (2002). In Section 3.3 we limited our study to two circular fields centred on the clusters. As extinction varies across the FOV for these two clusters, we have limited ourselves to stars from Slesnick et al. (2002) lying within these areas. The result is shown as Fig. 17. The difference of the median values of extinction using Q between the two positionally selected areas was found. The shift derived for h Per was $A_V = 0.157$ which has already been applied in Section 3.3. Therefore the reddening to χ Per only was needed, being $A_V = 1.571 \pm 0.079$.

4.1.2 NGC 2547, 2264 and Cep OB3b

For NGC 2547 we used the photometry of Claria (1982). The resulting median extinction value was 0.157 ± 0.008 mag. For NGC 2264 UBV member photometry from Mendoza & Gomez (1980) yielded a median $A_V = 0.371 \pm 0.0409$. The final field is Cep OB3b, where the photometry was from Jordi, Trullols & Galadi-Enriquez (1996), with a resulting median value of $A_V = 2.88 \pm 0.039$.

5 DATA COMPARISON

These data present an opportunity to make a qualitative assessment of how the PMS changes with age. To enable us to do this the sequences were shifted by the adopted distance moduli and extinctions (see Fig. 18). We selected four of our best sequences spanning as large an age range as possible. Data for NGC 2264 has been supplemented by photometry from Mendoza & Gomez (1980). They used

radial velocity to assign membership probabilities, and we plot only stars with membership probabilities of >90 per cent. This allowed us to plot the sequence members above $V_0 = 11$, where the stars are saturated in our catalogue.

5.1 Sequence spreads

The sequences in Fig. 18 appear to ‘crystallize’ with age. The absolute spread in CMD space of the sequences reduces as the age of the field increases. The trend appears to continue in the fields older than those presented in Fig. 18, with NGC 2547 ($\simeq 30$ Myr) showing a particularly clear sequence. Sequences older than 5 Myr do not appear to show large spreads. However, sequences younger than this show large spreads not explicable by photometric errors, variability and binarity, as shown in the case of Cep OB3b and σ Ori by Burningham et al. (2005a). This contrast with the Upper Sco-Cen OB association at $\simeq 5$ –6 Myr, which has an apparently wholly explicable photometric spread (Preibisch et al. 2002). It appears there is a change at about 5 Myr.

This suggests a possible cause of the anomalous spreads; namely accretion or infalling history. The half-life for accretion discs is estimated to be 3 Myr, therefore for low-mass objects one would expect the discs to have disappeared by $\simeq 6$ Myr (Haisch, Lada & Lada 2001; Oliveira et al. 2006). Accretion, from a disc increases the continuum luminosity along with various other effects, possibly pushing the stars blueward, resulting in a scatter both temporally older and younger (Tout, Livio & Bonnell 1999). This component of the spread would not be present in sequences older than $\simeq 6$ Myr. It should be noted however that this half-life is derived from the presence of dust; the half-life of gas within these discs is less certain.

An obvious alternative is that the groups are not co-eval. The time-scale of star formation itself must produce an intrinsic spread in age and hence in position in the CMD. In addition there is strong evidence for the episodic star formation within a group, subgroup, cluster or association. Thus another explanation for the secular evolution of the sequence spreads we observe in Fig. 18 could be an initial age spread evolving to older ages and the absolute spread therefore reducing as the isochrones bunch up in CMD space, that is, $d(\text{age})/dV$ increases. If the spread within the CMD is due to a genuine age spread, since our empirical isochrones are based on median magnitudes they will be biased towards younger ages.

5.2 Evidence for a gap in a $V, V - I$ CMD

The ONC has a discernible gap between the PMS stars and the MS stars, at the point where the PMS isochrone meets the zero-age main-sequences (ZAMS). This can be seen clearly in Fig. 18. There also appears to be a gap, again where the PMS meets the MS in h and χ Per and NGC 2264 (Fig. 18). A gap is evident in the photometry for NGC 6530 and perhaps IC 5146 (see Figs 13 and 12). A further excellent example of the gap can be seen in the CMD of NGC 4755 in Lyra et al. (2006).

To ascertain whether this gap between MS and PMS stars is a general feature we used the isochrones to find the position (in CMD space) of the PMS–MS connection. In some of our younger fields the gap is situated around our bright magnitude limit. In these cases we cannot be sure of the gap’s existence. There is however a discernible dearth of members at the head of the PMS, which can be seen in Cep OB3b, σ Ori, IC 348, NGC 2362 and λ Ori. This explains the general shape of many CMDs of PMS regions, which appear to consist of a sequence parallel and redward of the contamination which disappears at brighter magnitudes. The brightest stars at the

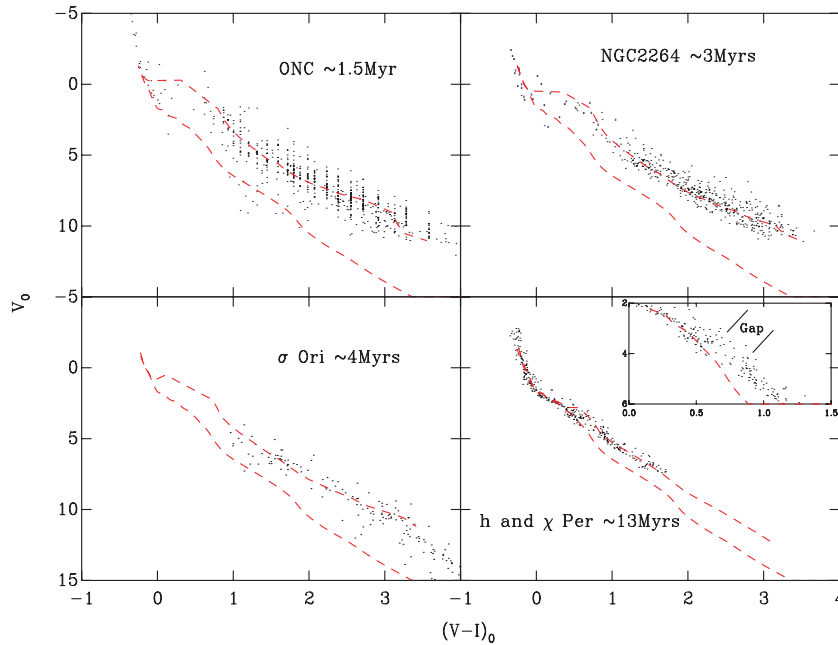


Figure 18. The likely PMS objects for fields of different ages, plotted in dereddened colours and absolute magnitudes. The spread in absolute colour magnitude space clearly decreases as age increases. The ZAMS and isochrones of approximately the correct age from Siess et al. (2000) are shown.

head of this sequence must represent the top of the PMS, with the MS appearing blueward of this. The MS, and therefore the gap, is often obscured by contamination.

We could not definitively detect the gap in NGC 7160 or 2547. In the case of NGC 7160 the gap would fall in an area devoid of membership information. Finally, for our oldest field NGC 2547 the PMS and MS isochrones lie very close together meaning the gap, if present, would be very small compared to the younger fields.

It is apparent that this phenomenon occurs in all data sets where we would expect to observe it. This feature delineates the transition from PMS to MS, hence Stolte et al. (2004) call this the PMS/MS transition region (they identified it in a $J_s, J_s - K_s$ CMD of NGC 3603). We prefer the term radiative convective (R-C) gap as we feel this emphasizes the physics involved which we outline in the next section.

5.3 The origin of R-C gap

From the theoretical isochrones an explanation for this gap becomes apparent (see Fig. 19). Physically the R-C gap is the transition phase of stars from a fully convective object to the development of a radiative core. The Hayashi tracks which the lower mass PMS stars descend in CMD space represent the gravitational contraction of a fully convective object. As the star heats and the core density gradually increases, at some stage the core becomes radiative, and the track changes to a Henyey track which is almost horizontal in a $V/V - I$ CMD. For massive stars this happens earlier in the star's evolution than for low-mass stars (Collins 1989); a $7 M_{\odot}$ star will develop a radiative core almost immediately.

The development and evolution of the radiative core causes the separation of the PMS and MS. As the transition proceeds the mass tracks are almost parallel with the isochrones, meaning evolution across the area of CMD space between the PMS and MS is rapid compared to the descent down the Hayashi tracks. The difference in motion in CMD space is clearly demonstrated in Fig. 19. Here

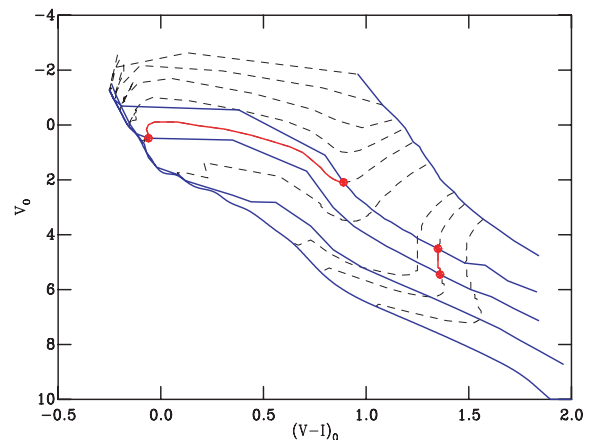


Figure 19. Isochrones (solid blue lines) from Siess et al. (2000) for the approximate ages of the four fields in Fig. 18; 1, 3 and 13 Myr. Mass tracks (dashed lines) are shown for 7, 6, 5, 4, 3, 2, 1.2, 1.0 and $0.8 M_{\odot}$. The evolution between 1 and 3 Myr of 3 and $1 M_{\odot}$ stars are shown as filled circles, with the track highlighted in red.

the distance between a 1- and 3-Myr isochrone for a star on a fully convective track is small when compared to a star at the head of the PMS which will have joined the MS by 3 Myr, moving much farther in CMD space. This means at any given age a sequence should have a relative sparsity of stars in this gap compared to the slowly evolving PMS and almost stationary MS (on these time-scales).

As is visible from the data in Fig. 18 and the theory in Fig. 19 the size of the dislocation between the MS and PMS is a function of age. For the younger fields the PMS lies far from the MS and the transition occurs at high masses. The higher the mass of a star the earlier the formation of a radiative core and the sooner it changes to a Henyey track. Higher mass objects move to the MS more swiftly along these tracks. The reverse is also true. As the field becomes

older, the mass at which the core develops falls and the evolution of the star progresses more slowly.

The age dependency of the size of the gap has important ramifications. If it is possible to identify the head of the PMS and the MS members for a given field, the separation of these will be a distance and reddening independent measure of the age. There are several restrictions. If the field is older than around 15 Myr the gap becomes too small to detect reliably. The gap may also lie within an area of high contamination, meaning many objects will need to be assessed for membership to be certain of detecting the gap. In some cases variable extinction will prevent photometric detection of the gap, as the relative positions of the stars shift in a CMD; in these cases individual extinctions will need to be found. As the size of the gap depends critically on the formation and growth of the radiative core, it may also represent an excellent test of the stellar interior models.

6 RELATIVE AGES

The sequences displayed in Fig. 18 are the results after membership selection. To create a relative age ladder however the sequences must appear on the same CMD, superimposed over one another. Such a figure would be confused due to the number of points and the spreads of the sequences. Therefore at this stage we move to representing the sequences by the spline fits. To aid analysis we also created a ZAMS subtracted CMD, using the ZAMS relation of Siess, Dufour & Forestini (2000). In these diagrams the points on the spline fits each have the $V - I$ of the MS star at equivalent V subtracted from their $V - I$. This separates the sequences much more clearly. Fig. 20 shows a sample of the empirical isochrones.

The disadvantage of the ZAMS subtraction process is that it enhances the residuals of the spline fitting procedure. As can be seen in Fig. 21 at the R-C gap there is a dearth of data which causes the spline fit to degrade. This also causes the fit to the MS after the R-C gap to be poor as the spline fits enforce a gradient continuity criterion. These residuals have been acceptable (if noted) until now

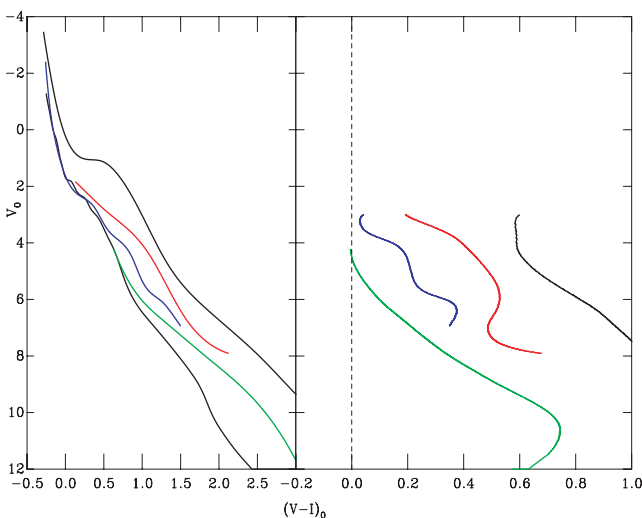


Figure 20. A sample of the empirical isochrones. Youngest to oldest, the ONC, NGC 7160, h and χ Per and NGC 2547. The left-hand panel is the empirical isochrones in an absolute V , $V - I$ CMD, with the lowest curve the ZAMS relation of Siess et al. (2000). The right-hand panel is the ZAMS subtracted space; at a given V the ZAMS $V - I$ is subtracted from the $V - I$ of the spline. The vertical dashed line shows the position of the ZAMS.

but are greatly magnified in the ZAMS subtracted space. Therefore we have cut the splines in ZAMS subtracted space at a $V_0 = 3$.

6.1 Theory comparison

It is useful at this stage to compare the empirical isochrones we have created to their theoretical counterparts. Although we have used isochrones from Siess et al. (2000), the effects described are apparent with all the other isochrones we have examined, though a complete investigation of all the models lies outside the scope of this paper.

We have adopted an approximately solar metallicity, $Z = 0.02$. James et al. (2006) shows that for a number of star-forming regions the metallicity is slightly subsolar, it is also likely that different clusters, associations, groups or subgroups will have differing compositions. Therefore it is pertinent to ask what age difference would be obtained by fitting a higher or lower metallicity isochrone to our representative sequence of 3 Myr. If we compare a 3 Myr $Z = 0.02$ isochrone with isochrones of $Z = 0.01$ and 0.04 the closest matches have approximate ages of 2.2 and 3.5 Myr, respectively. Thus changes in the metallicity by a factor of 2 are too small to affect the discussion which follows.

In Fig. 20 we can see a minor problem. NGC 2547 can be seen to cut across the younger sequences, this is probably due to observations being made using a different I filter (see Section 2.3) coupled with the fact that the reddest standard is at a $V - I$ of 2.5 in this case, exaggerated by the ZAMS subtraction process.

In addition, our comparison reveals three serious concerns. (i) Figs 18 and 21 show that whilst an acceptable fit to the theoretical isochrones can be obtained over most of the sequence, the model isochrone lies above the data at the boundaries of the R-C gap for NGC 2264 and h and χ Per. Furthermore, the MS members overlap the PMS in magnitude space for all our fields, in direct contradiction to the isochrones, assuming a coeval population (see Section 9 for a further discussion of this). (ii) For younger sequences a theoretical isochrone fitted to the PMS is a poor match to the MS. (iii) Although the young sequences have a large scatter, the PMS isochrones fail to consistently follow the centre of this spread. For example, in the NGC 2264 most stars lie above the isochrone at $V - I > 1$, but below it at $V - I < 1$. The conclusion is that when fitting isochrones to sequences across a limited colour range, one must be aware that the fit will not necessarily be good across the rest of the sequence. This implies that the age derived depends on which part of the sequence is fitted. This is why empirical isochrones are potentially superior to their theoretical counterparts.

6.2 Selecting the fiducial sequences

As we shall see later, we can roughly group the youngest objects into three groups with ages of 1, 3 and 5 Myr. The sequences older than this are much more clearly separated. These three groups are separated in age such that using the maximum uncertainty in distance modulus (typically 0.2 mag) could shift a sequence by one group, older or younger. For use as fiducial sequences we select the spline curves of one sequence from each group, typifying the group. We preferentially select the sequence from each group with the most certain distance and age. These fiducial isochrones can then be used to derive relative ages to further fields, with selection of the fiducials guided by the sequence's placement in colour-magnitude space. The group at around 5 Myr is problematic, as discussed later it contains only two clusters σ Ori and IC 348; σ Ori has an uncertain distance. However, IC 348 is found to be much older (in this work) than the

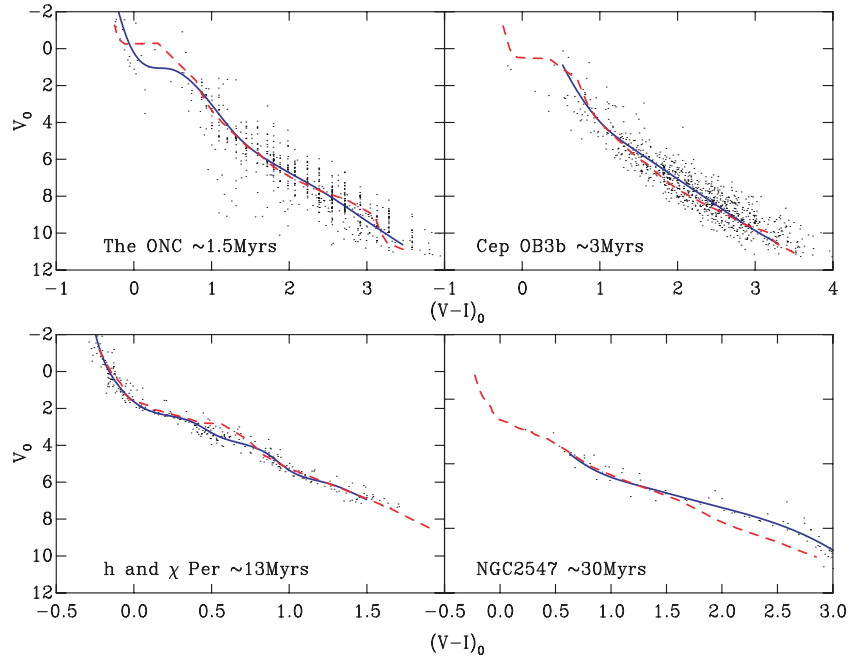


Figure 21. The selected members for the ONC, Cep OB3b, h and χ Per and NGC 2547. The solid line is the empirical isochrone. The dashed line is the best-fitting isochrone (by eye) from Siess et al. (2000) ($\simeq 1.5$, $\simeq 3$, $\simeq 13$ and $\simeq 16$ Myr, respectively). The sequences and empirical isochrones can be seen to move away from the theoretical counterparts to varying degrees.

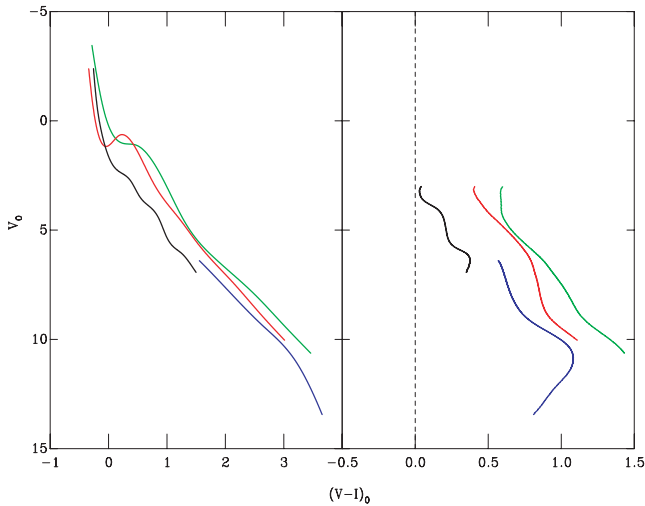


Figure 22. The selected fiducial sequences; h and χ Per, σ Ori, NGC 2264 and the ONC. The vertical dashed line shows the position of the ZAMS.

age given in the literature. Therefore σ Ori has been chosen as the fiducial for this group, despite its large distance uncertainty.

The fiducial empirical isochrones selected were the ONC, NGC 2264, σ Ori and h and χ Per, with assumed ages (from the literature or fitting of Siess et al. (2000) isochrones) of 1, 3, 4 and 13 Myr. These fiducials will be used in Section 7. The fiducials are shown in Fig. 22.

7 USING A RELATIVE AGE LADDER

We can now use our age ladder to determine relative ages for several fields. Throughout the figures in this section the fiducial isochrones

are marked as dashed lines, with the subject sequence appearing as a solid line.

7.1 Cep OB3b

For Cep OB3b the membership list has been discussed in Section A6 and the CMD with the members overlaid is shown as Fig. A3. Estimates for the distance modulus are from Section B18 and the extinction from Section 4.1.2.

We use the spline fit to the data (Section 3.2), overlaid on the fiducial isochrones from Section 6.2 to age the subgroup. This reveals an interesting result. The subgroup Cep OB3b can clearly be seen to lie on the same locus as NGC 2264, with σ Ori being slightly older, implying an age for Cep OB3b of $\simeq 3$ Myr (Fig. 23). The best

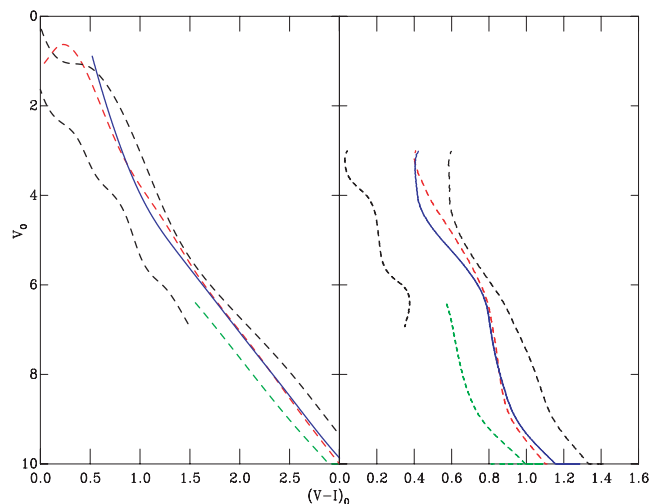


Figure 23. The fitted sequence for Cep OB3b (solid line). NGC 2264, h and χ Per, σ Ori and the ONC are shown as dashed lines for reference.

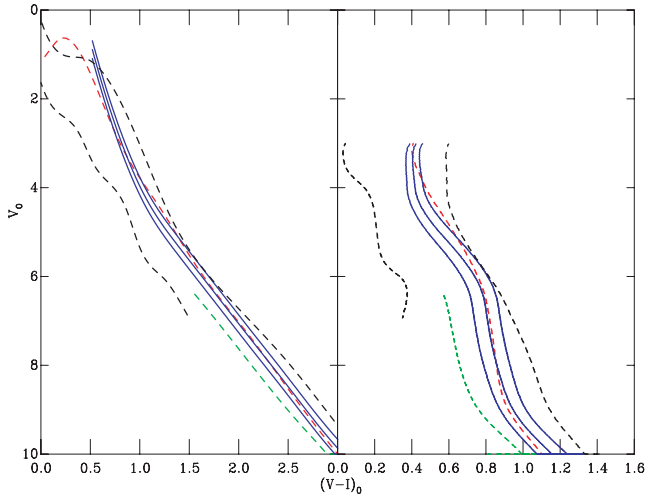


Figure 24. The sequence for Cep OB3b assuming three different distance moduli (solid lines). NGC 2264, h and χ Per, σ Ori and the ONC are shown as dashed lines for reference.

previous age estimate for this subgroup is Jordi et al. (1996) at 5.5 Myr. The older estimate would have made Cep OB3b the oldest group to contain molecular material. We therefore conclude that the lower age of 3 Myr is more likely. The distance modulus uncertainty range is ± 0.20 mag. The effect of this can be seen in Fig. 24, where the relative position of Cep OB3b does not change dramatically even when the entire uncertainty budget is used. In addition, the photometry shown in Fig. A3 reveals evidence for an R–C gap at the head of the PMS in a position similar to that of NGC 2264 at an age of $\simeq 3$ Myr, also suggesting a similar age for the two groups.

7.2 IC 348

Using our relative age system, as in Section 7.1 we found IC 348 to have an age between that of σ Ori and NGC 2264. The empirical isochrone therefore suggests that the cluster is somewhat older than NGC 2264 and indeed Cep OB3b. This can be seen in Fig. 25. This contrasts with the literature age of 2–3 Myr (e.g. Haisch et al. 2001). To obtain an age of 3 Myr or less would require a shift of $\simeq 0.5$ mag in

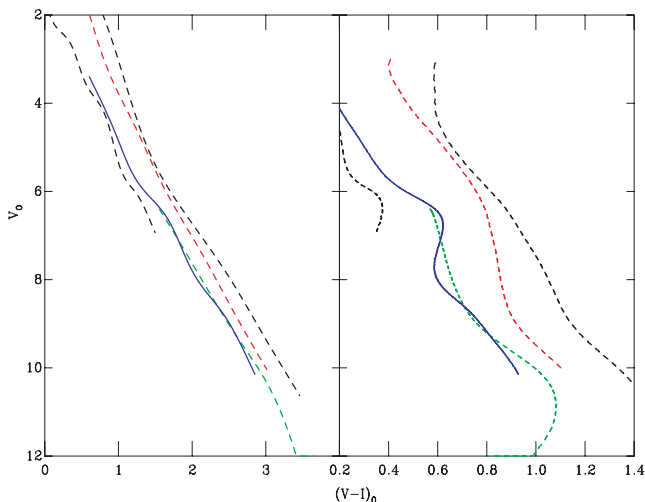


Figure 25. The fitted sequence for IC 348 (solid line). h and χ Per, σ Ori, NGC 2264 and the ONC are shown as dashed lines for reference.

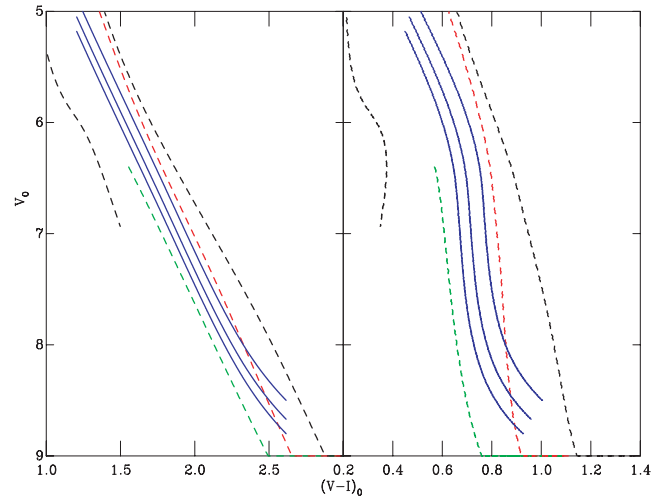


Figure 26. The sequence for λ Ori assuming the distance moduli from Dolan & Mathieu (2001), Murdin & Penston (1977) and *HIPPARCOS* (solid lines). The ONC, NGC 2264, σ Ori and h and χ Per are shown as dashed lines for reference.

the distance modulus, yet the uncertainties in the distance modulus to IC 348 are significantly smaller than this, $-0.16/+0.14$ mag (see Appendix B).

7.3 λ Ori

Fig. 26 shows the fiducial sequence plot with λ Ori placed at distance moduli of 7.77, 7.90 and 8.07 mag, representing the limits of the *HIPPARCOS* measurement. Fig. 26 shows λ Ori is largely degenerate with NGC 2264, and therefore has an age of $\simeq 3$ Myr. This is certainly consistent with the MS turn-off age of 4 Myr derived from UBV photometry by Murdin & Penston (1977) but not with the age of 6–7 Myr derived by Dolan & Mathieu (2001) using narrow-band photometry of high-mass stars).

7.4 NGC 2362

The relative age plot can be seen in Fig. 27. Here NGC 2362 appears between NGC 2264 and σ Ori, giving it an age of 3–4 Myr. This is consistent with the ages derived by Dahm (2005) of $\simeq 1.8$ Myr using the isochrones of D’Antona & Mazzitelli (1997), and 3.5–5 Myr from the isochrones of Baraffe et al. (1998). However, the shift in distance modulus to achieve an age of greater than 4 Myr would be $\simeq 0.4$ mag; larger than the typical distance modulus uncertainty.

7.5 IC 5146

The age plot is displayed as Fig. 28. IC 5146 appears to have an age approximately equal to that of the ONC. The median age found by Herbig & Dahm (2002) is $\simeq 1$ Myr, agreeing with our result.

7.6 NGC 6530

Photometry from this cluster is taken from Prisinzano et al. (2005). They only provide photometry of stars which are also in the catalogues of Walker (1957) or Kilambi (1977) or matched to an X-ray

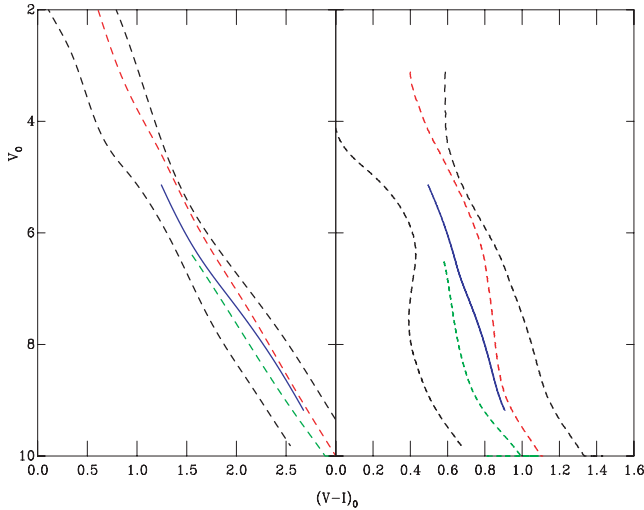


Figure 27. The fitted sequence for NGC 2362 (solid line). The ONC, NGC 2264, σ Ori and h and χ Per are shown as dashed lines for reference.

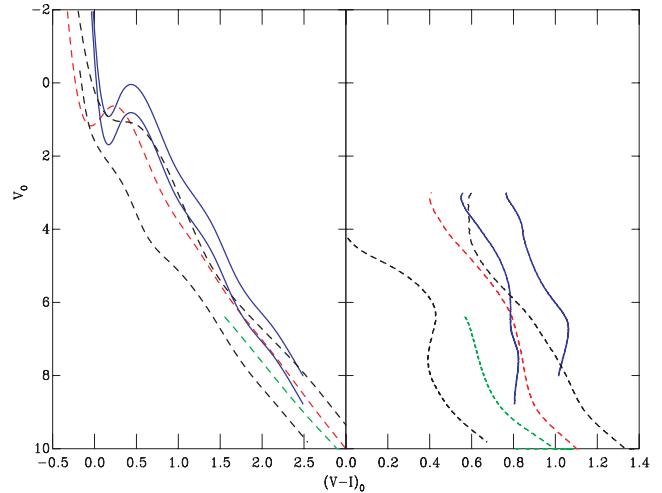


Figure 29. The fitted sequence for NGC 6530 (solid line). The ONC, NGC 2264, σ Ori and h and χ Per are shown as dashed lines for reference.

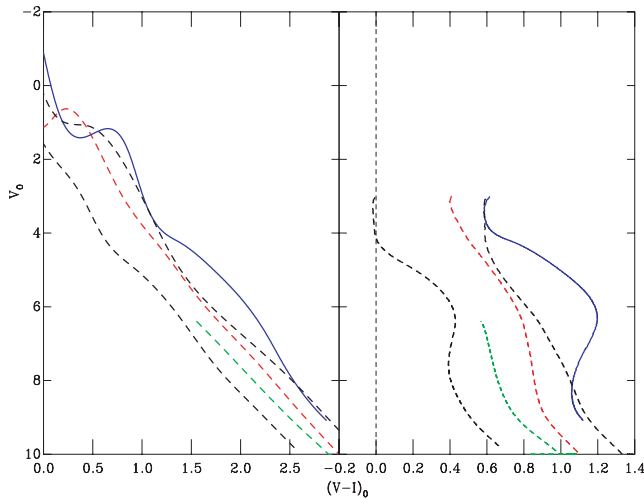


Figure 28. The fitted sequence for IC 5146 (solid line), assuming the distance modulus from Herbig & Dahm (2002). The ONC, NGC 2264, σ Ori and h and χ Per are shown as dashed lines for reference. The vertical dashed line shows the position of the ZAMS.

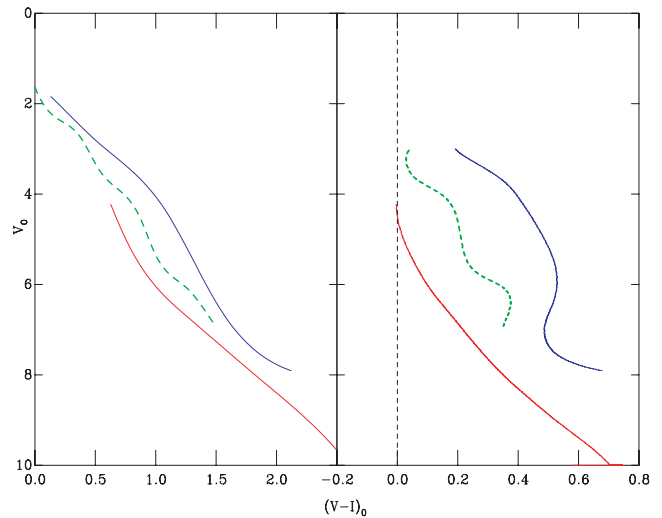


Figure 30. The fitted sequences (solid lines) for (younger to older); NGC 7160 (blue, ≈ 10) and NGC 2547 (red, ≈ 30 –45 Myr). The dashed line is the spline curve for h and χ Per (≈ 13 Myr). The vertical dashed line shows the position of the ZAMS

source from Damiani et al. (2004), and are brighter than $V = 18$. Prisinzano et al. (2005) use the isochrones of Siess et al. (2000) fitted to PMS stars to obtain a median age of 2.3 Myr. Sung, Chun & Bessell (2000) find an age of 1.5 Myr from fitting isochrones to an $H\alpha$ selected PMS after conversion to a Hertzsprung–Russell diagram. Damiani et al. (2004), using X-ray selection and the photometry of Sung et al. (2000) find an age of 0.5–1.5 Myr. As for previous fields this spline has been overlaid on the fiducial diagram seen as Fig. 29. Two distance moduli are displayed, that of Prisinzano et al. (2005) ($d_m \approx 10.48$ mag) and that of Sung et al. (2000) ($d_m = 11.25 \pm 0.1$ mag). The sequence in Fig. 29 appears to lie above the ONC for the greater distance modulus and coincident, or perhaps just below, the ONC, for the lower distance modulus. Suggesting an age of < 1 Myr at the further distance or ≈ 1 –2 Myr for the closer distance. Thus we cannot differentiate between the literature ages.

7.7 NGC 7160 and 2547

These clusters have older age estimates than the fields aged using our earlier fiducial selection (Section 6.2). NGC 7160 has an age estimate of ≈ 10 Myr from isochrone fitting from Sicilia-Aguilar et al. (2005). NGC 2547 has age estimates varying from 30–45 Myr from MS isochrone fitting in Naylor et al. (2002) and the lithium depletion boundary in Jeffries & Oliveira (2005). Therefore we plot these empirical isochrones in Fig. 30 with h and χ Per as our only useful fiducial. NGC 7160 is clearly younger than h and χ Per, making the current age estimates reasonable. NGC 2547 cuts across the other sequences at redder $V - I$. This could be a problem with the standard calibrations, which extends only to a $V - I$ of 2.5 in the NGC 2547 reduction.

8 IMPLICATIONS OF THE REVISED AGES

The consequences of our revision of the relative ages of IC 348, NGC 2264, 2362 and the ONC are particularly pertinent to recent studies in two areas. First one is in gyrochronology. Large-sample rotation studies now exist for a subset of young clusters and from these a conventional view of the rotational evolution of stars between 1 and 5 Myr is developing. The rotational period distribution of the ONC is strongly bimodal. This distribution is believed to evolve into a unimodal distribution such as that of NGC 2264 and 2362. IC 348 has a distribution of rotation rates similar to that of the ONC, and yet we find it to be older than NGC 2264. This clearly raises a concern for the universality of any evolutionary model.

The second area our findings affect is the field of disc evolution. Haisch et al. (2001) plot the fraction of *JHKL* excess sources, used to infer a disc fraction as a function of age for different clusters or groups. This plot reveals a clear decrease in the inferred disc fraction with time. However, from this work two clusters, IC 348 and NGC 2264 should be relocated within this plot leading to a change in the finer structure of the trend at younger ages. The disc fractions for the ONC, IC 348, NGC 2264 and 2362 are $\simeq 80$, $\simeq 65$, $\simeq 52$ and $\simeq 12$ per cent, respectively. The relative age order of these four clusters found in this work (youngest to oldest) is the ONC, NGC 2264, 2362 and IC 348. Therefore they do not show a secular decline in disc fraction. This is illustrated most clearly by the Fig. 31, showing the disc fraction as a function age from Haisch et al. (2001) and as a function of the nominal ages found in this work.

Interestingly, IC 348 is out of place in rotation rate and disc evolution. If disc evolution drives the rotational evolution, say through disc locking, this is perhaps unsurprising. The key here may be the local environment. There are no O-stars associated with IC 348. NGC 2362 however has 6 O-stars stars designated as cluster members, the ONC has 16 and NGC 2264 13 (Maíz-Apellániz et al. 2004). This supports the idea that a larger fraction of the PMS stars in IC 348 have retained discs due to the absence of winds and/or ionizing radiation from massive stars. Our relative ages may, therefore, be amongst the first indications of the importance of environment on disc and rotation rate evolution (see also Stolte et al. 2004).

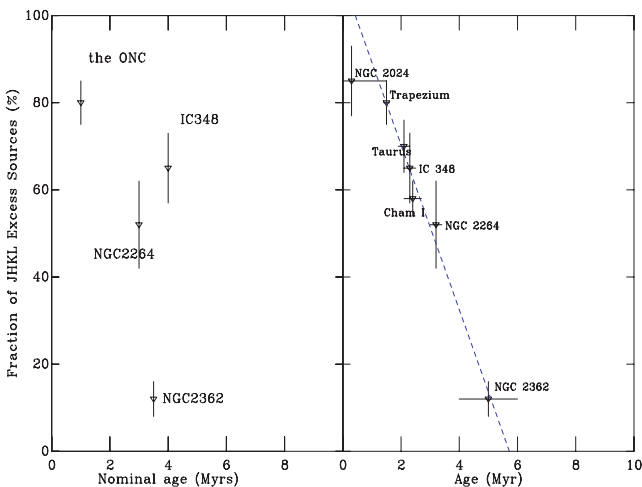


Figure 31. Fraction of *JHKL* excess sources, used a disc indicator for the ONC, IC 348, NGC 2264 and 2362 from Haisch et al. (2001); left-hand panel: against nominal ages found in this work; right-hand panel: against cluster ages used in Haisch et al. (2001). The straight line is a simple linear regression fit.

An alternative explanation has been put forward in Lyo et al. (2003) by indentifying NGC 2362 as anomalous. Lyo et al. (2003) suggest this could be due to an incorrect age determination; this is ruled out is by this work. They also suggest it could be an artefact of the poor limiting magnitude achieved when using the *L* band, meaning this band is very sensitive to distance and provides a disc fraction derived from a different mass range for clusters at an unequal distance. Therefore any conclusions reached on the secular trends of disc fractions must be tentative, due to the heterogeneous nature of the stellar mass range used.

9 CONCLUSIONS

We have presented photometry for a large selection of young stellar populations in differing environments. The selection criteria and some of the photometry is heterogeneous and from many literature sources. Despite these difficulties this attempt at producing a self-consistent set of empirical isochrones has been largely successful. We have characterized and fitted the sequences in CMD space, and grouped the sequences by position in the CMD – effectively age. Then using the clearest sequences typifying each group, a relative age ladder was developed for use with additional sequences. Our final groupings for all the sequences we have data for were as follows.

- (i) $\simeq 1$ Myr; the ONC, NGC 6530 and IC 5146.
- (ii) $\simeq 3$ Myr; Cep OB3b, NGC 2362, λ Ori and NGC 2264.
- (iii) $\simeq 4$ –5 Myr; σ Ori and IC 348.
- (iv) $\simeq 10$ Myr; NGC 7160 – uncertain due to lack of members.
- (v) $\simeq 13$ Myr; h and χ Per.
- (vi) $\simeq > 30$ Myr; NGC 2547.

The distance moduli remain the largest source of uncertainty, allowing the possibility of changing a sequence by plus or minus one group in age. Cep OB3b is thus somewhat younger than previously thought, and IC 348 somewhat older. Both the disc fraction and rotation-period distribution for IC 348 imply it is younger than our derived age. Since, in contrast to the other regions we have studied IC 348 has no O-stars, this suggests that the winds and/or ionizing radiation from these stars have a significant effect of accretion disc evolution.

The data also allow us to follow the feature in the CMD we term the R–C gap. In most CMDs this feature appears as a gap between the PMS and MS members, or as a dearth of members at the head of the PMS in some younger sequences. We have been able to trace the evolution of the gap from 1 Myr through to the intermediate age (in the context of these data) clusters of h and χ Per. We have explored the physics behind the appearance of a gap in the *V*, *V* – *I* sequences and the evolution of the gap with age. It is encouraging that the size of the gap, where it is visible, follows the same age ordering as found using the empirical isochrones. Further to this we have touched upon the possibility of using the size of the R–C gap as a distance and extinction independent age indicator.

The R–C gap could also be used as a powerful tool to calculate age spreads within a sequence. If one could account for all possible forms of spread within a CMD, and had memberships and spectral types/masses for all stars at the boundaries of the R–C gap. By finding the lowest mass star to have already traversed the R–C gap, and then finding the youngest star (via isochrones) of the same mass on the PMS one could calculate an age spread.

Within this study is a limited investigation of the fit across sequences of theoretical isochrones. We conclude that isochrone formulations are self-consistent when applied within a restricted mass

or colour range not bridging the R–C gap. They tend to become less reliable when we have attempted to fit both the MS and PMS, that is, both sides of the R–C gap, excluding the intermediate age clusters, h and χ Per. Most recent studies in the literature concentrate on either the turn-on region of a sequence or the low-mass sections, meaning that the inconsistency of the fits is not always apparent.

Finally, we tentatively suggest a critical change in the nature of spreads within a CMD at $\simeq 5$ Myr. Above $\simeq 5$ Myr the sequence members are generally not associated with molecular material and have wholly explicable photometric spreads. Below $\simeq 5$ Myr the sequence members are often associated with molecular material and show inexplicably large photometric spreads.

To revisit these or other clusters with a larger photometric study applying the same mechanisms as in this paper would be beneficial and we believe could provide a benchmark collection of empirical isochrones for comparison to theory. In unison with this a comprehensive study of the application and limitations of the R–C gap as an age indicator would be a logical next step.

ACKNOWLEDGMENTS

NJM is funded by a UK particle physics and astronomy research council (PPARC) studentship. The INT is operated on the island of La Palma by the Isaac Newton Group in the Spanish Observatorio del Roque de los Muchachos of the Instituto de Astrofísica de Canarias. This publication makes use of data products from the 2MASS, which is a joint project of the University of Massachusetts and the Infrared Processing and Analysis Center/California Institute of Technology, funded by the National Aeronautics and Space Administration and the National Science Foundation. We would also like to thank S. Dahm and G. Herbig for the provision of extra data.

REFERENCES

Balona L. A., Laney C. D., 1996, *MNRAS*, 281, 1341
 Baraffe I., Chabrier G., Allard F., Hauschildt P. H., 1998, *A&A*, 337, 403
 Béjar V. J. S., Zapatero Osorio M. R., Rebolo R., 1999, *ApJ*, 521, 671
 Blaauw A., Hiltner W. A., Johnson H. L., 1959, *ApJ*, 130, 69
 Bonatto C., Bica E., Girardi L., 2004, *A&A*, 415, 571
 Brown A. G. A., de Geus E. J., de Zeeuw P. T., 1994, *A&A*, 289, 101
 Burningham B., Naylor T., Jeffries R. D., Devey C. R., 2003, *MNRAS*, 346, 1143
 Burningham B., Naylor T., Littlefair S. P., Jeffries R. D., 2005a, *MNRAS*, 363, 1389
 Burningham B., Naylor T., Littlefair S. P., Jeffries R. D., 2005b, *MNRAS*, 356, 1583
 Capilla G., Fabregat J., 2002, *A&A*, 394, 479
 Claria J. J., 1982, *A&AS*, 47, 323
 Cohen R. E., Herbst W., Williams E. C., 2004, *AJ*, 127, 1602
 Collins G. W., 1989, *The Fundamentals of Stellar Astrophysics*. Freeman & Co., New York, p. 512
 Dahm S. E., 2005, *AJ*, 130, 1805
 Dahm S. E., Simon T., 2005, *AJ*, 129, 829
 Damiani F., Flaccomio E., Micela G., Sciortino S., Harnden F. R., Murray S. S., 2004, *ApJ*, 608, 781
 D'Antona F., Mazzitelli I., 1997, *Memorie della Societa Astronomica Italiana*, 68, 807
 Diplias A., Savage B. D., 1994, *ApJS*, 93, 211
 Dolan C. J., Mathieu R. D., 2001, *AJ*, 121, 2124
 Flaccomio E., Micela G., Sciortino S., Favata F., Corbally C., Tomaney A., 1999, *A&A*, 345, 521
 Flaccomio E., Damiani F., Micela G., Sciortino S., Harnden F. R., Murray S. S., Wolk S. J., 2003, *ApJ*, 582, 398
 Genzel R., Reid M. J., Moran J. M., Downes D., 1981, *ApJ*, 244, 884

Getman K. V., Feigelson E. D., Townsley L., Broos P., Garmire G., Tsujimoto M., 2006, *ApJS*, 163, 306
 Gullbring E., Hartmann L., Briceno C., Calvet N., Muzerolle J., 1998, in Donahue R. A., Bookbinder J. A., eds, *ASP Conf. Ser. Vol. 154, Cool Stars, Stellar Systems, and the Sun*. Astron. Soc. Pac., San Francisco, p. 1709
 Haisch K. E. Jr, Lada E. A., Lada C. J., 2001, *ApJ*, 553, L153
 Hartmann L., 1998, in Hartmann L., ed., *Cambridge Astrophysics Ser. Vol. 32, Accretion Processes in Star Formation*. Cambridge Univ. Press, Cambridge, New York, ISBN 0521435072
 Herbig G. H., 1998, *ApJ*, 497, 736
 Herbig G. H., Dahm S. E., 2002, *AJ*, 123, 304
 Herbst W., Bailer-Jones C. A. L., Mundt R., Meisenheimer K., Wackermann R., 2002, *A&A*, 396, 513
 Hillenbrand L. A., 1997, *AJ*, 113, 1733
 James D. J., Melo C., Santos N. C., Bouvier J., 2006, *A&A*, 446, 971
 Jeffries R. D., Oliveira J. M., 2005, *MNRAS*, 358, 13
 Jeffries R. D., Tolley A. J., 1998, *MNRAS*, 300, 331
 Jeffries R. D., Maxted P. F. L., Oliveira J. M., Naylor T., 2006, *MNRAS*, 371, L6
 Johnson H. L., Morgan W. W., 1953, *ApJ*, 117, 313
 Jordi C., Trullols E., Galadí-Enriquez D., 1996, *A&A*, 312, 499
 Kenyon M. J., Jeffries R. D., Naylor T., Oliveira J. M., Maxted P. F. L., 2005, *MNRAS*, 356, 89
 Kilambi G. C., 1977, *MNRAS*, 178, 423
 Lamm M. H., Bailer-Jones C. A. L., Mundt R., Herbst W., Scholz A., 2004, *A&A*, 417, 557
 Lamm M. H., Mundt R., Bailer-Jones C. A. L., Herbst W., 2005, *A&A*, 430, 1005
 Landolt A. U., 1992, *AJ*, 104, 340
 Littlefair S. P., Naylor T., Burningham B., Jeffries R. D., 2005, *MNRAS*, 358, 341
 Luhman K. L., 1999, *ApJ*, 525, 466
 Luhman K. L., Stauffer J. R., Muench A. A., Rieke G. H., Lada E. A., Bouvier J., Lada C. J., 2003, *ApJ*, 593, 1093
 Luhman K. L., Lada E. A., Muench A. A., Elston R. J., 2005a, *ApJ*, 618, 810
 Luhman K. L., McLeod K. K., Goldenson N., 2005b, *ApJ*, 623, 1141
 Lyo A.-R., Lawson W. A., Mamajek E. E., Feigelson E. D., Sung E.-C., Crause L. A., 2003, *MNRAS*, 338, 616
 Lyra W., Moitinho A., van der Blik N., Alves J., 2006, *A&A*, 453, 101
 Maíz-Apellániz J., Walborn N. R., Galué H. Á., Wei L. H., 2004, *ApJS*, 151, 103
 Marco A., Bernabeu G., 2001, *A&A*, 372, 477
 Mendoza V. E. E., Gomez T., 1980, *MNRAS*, 190, 623
 Moitinho A., Alves J., Huéramo N., Lada C. J., 2001, *ApJ*, 563, L73
 Moreno-Corral M. A., Chavarría K. C., de Lara E., Wagner S., 1993, *A&A*, 273, 619
 Muminov M., 1996, *VizieR Online Data Catalog*, 5027, 0
 Murdin P., Penston M. V., 1977, *MNRAS*, 181, 657
 Naylor T., 1998, *MNRAS*, 296, 339
 Naylor T., Fabian A. C., 1999, *MNRAS*, 302, 714
 Naylor T., Totten E. J., Jeffries R. D., Pozzo M., Devey C. R., Thompson S. A., 2002, *MNRAS*, 335, 291
 Ogura K., Sugitani K., Pickles A., 2002, *AJ*, 123, 2597
 Oliveira J. M., Jeffries R. D., van Loon J. T., Rushton M. T., 2006, *MNRAS*, 369, 272
 Park B.-G., Sung H., Bessell M. S., Kang Y. H., 2000, *AJ*, 120, 894
 Perez M. R., The P. S., Westerlund B. E., 1987, *PASP*, 99, 1050
 Pinsonneault M. H., Terndrup D. M., Hanson R. B., Stauffer J. R., 2004, *ApJ*, 600, 946
 Pozzo M., Naylor T., Jeffries R. D., Drew J. E., 2003, *MNRAS*, 341, 805
 Preibisch T., Feigelson E. D., 2005, *ApJS*, 160, 390
 Preibisch T., Zinnecker H., 2002, *AJ*, 123, 1613
 Preibisch T., Brown A. G. A., Bridges T., Guenther E., Zinnecker H., 2002, *AJ*, 124, 404
 Prisinzano L., Damiani F., Micela G., Sciortino S., 2005, *A&A*, 430, 941
 Robichon N., Arenou F., Mermilliod J.-C., Turon C., 1999, *A&A*, 345, 471

- Sanner J., Altmann M., Brunzendorf J., Geffert M., 2000, *A&A*, 357, 471
 Sanz-Forcada J., Franciosini E., Pallavicini R., 2004, *A&A*, 421, 715
 Sherry W. H., Walter F. M., Wolk S. J., 2004, *AJ*, 128, 2316
 Sicilia-Aguilar A., Hartmann L. W., Briceño C., Muzerolle J., Calvet N., 2004, *AJ*, 128, 805
 Sicilia-Aguilar A., Hartmann L. W., Hernández J., Briceño C., Calvet N., 2005, *AJ*, 130, 188
 Siess L., Dufour E., Forestini M., 2000, *A&A*, 358, 593
 Slesnick C. L., Hillenbrand L. A., Massey P., 2002, *ApJ*, 576, 880
 Stauffer J. R., Jones B. F., Backman D., Hartmann L. W., Barrado y Navascués D., Pinsonneault M. H., Terndrup D. M., Muench A. A., 2003, *AJ*, 126, 833
 Stolte A., Brandner W., Brandl B., Zinnecker H., Grebel E. K., 2004, *AJ*, 128, 765
 Straizys V., Kuriliene G., 1981, *Ap&SS*, 80, 353
 Strom S. E., Strom K. A., Carrasco L., 1974, *PASP*, 86, 798
 Sung H., Bessell M. S., Lee S., 1997, *AJ*, 114, 2644
 Sung H., Chun M.-Y., Bessell M. S., 2000, *AJ*, 120, 333
 Tout C. A., Livio M., Bonnell I. A., 1999, *MNRAS*, 310, 360
 Uribe A., García-Varela J., Sabogal-Martínez B., Higuera G. M. A., Brieva E., 2002, *PASP*, 114, 233
 Walker M. F., 1957, *ApJ*, 125, 636

APPENDIX A: LITERATURE MEMBERSHIPS

This section details the memberships for each field. Table 3 (above) shows the group, the data type and the reference for each of the groups in this section. Tables 4–29 may be found at http://www.astro.ex.ac.uk/people/timn/Catalogues/table_tables.html

A1 NGC 2264

The X-ray sources (Table 10) picked out a reasonably clear sequence (see Fig. A1), although there were also some X-ray active foreground and background objects. The spectroscopic members (Table 11) came from Dahm & Simon (2005) who selected members using $H\alpha$ strength from narrow-band imaging, a selection mechanism which is unbiased in colour–magnitude space. Spectroscopic observations were taken as follow-up. The periodic variables (Table 9) came from Lamm et al. (2004) and Lamm et al. (2005). We have used the entire periodic variable catalogue, whereas the final membership list of Lamm et al. (2005) imposed further isochrone

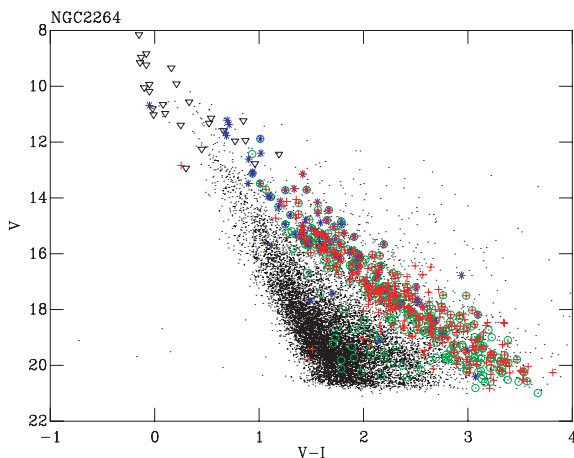


Figure A1. The full catalogue for the NGC 2264 field (dots). Circles are the periodic variables from Lamm et al. (2004), asterisks are X-ray sources from Flaccomio et al. (1999) and crosses are $H\alpha$ sources from Dahm & Simon (2005).

driven selection. Our photometry has been supplemented with the photometry for bright stars from Mendoza & Gomez (1980), as these stars were saturated in our catalogue. We include only those stars with probability of membership greater than 90 per cent from the proper motions of (Mendoza & Gomez 1980). We have also excluded W33; the anomalous photometry of this star was also noted in Mendoza & Gomez (1980). The full CMD with each form of membership criterion added is shown here as Fig. A1.

A2 NGC 2547

Jeffries & Oliveira (2005) carried out spectroscopy (Table 5) of a photometrically selected sample. The photometric sequence was clear of the contamination in this instance and so the colour–magnitude selection should not have produced a bias in the CMD space. Radial velocity (RV) was used to define cluster memberships. The presence of Li below the Li boundary was also used. The X-ray members (Table 4) are from Jeffries & Tolley (1998).

A3 ONC

Hillenbrand (1997) calculated extinctions for a subset of stars, using spectroscopic measurements of stars already identified as members from a range of literature sources, in a spatially selected region encompassing the inner 15 arcmin radius. We have used only those stars with spectroscopically calculated extinctions with assigned membership probabilities above 80 per cent. Periodic variables were from Herbst et al. (2002) and X-ray sources from Flaccomio et al. (2003).

A4 NGC 7160

Members were taken from Sicilia-Aguilar et al. (2004) and Sicilia-Aguilar et al. (2005) (Table 7). In these studies a photometric sample of stars was selected, initially by considering those lying above the 100-Myr isochrone in a $V, V-I$ CMD and lying within a magnitude range of $V = 15-19$ mag. A further selection was then made of stars with RI variability, then using U -band and 2MASS colours (biased to accreting stars). Spectroscopy was then used to measure extinctions and therefore assign memberships. The probability of membership was fixed to the distance in standard deviations (σ) from the average extinction value for the group. This relies on intrinsic colours. The members selected are those within 1σ of the average extinction.

A5 σ Ori

Spectroscopic members were taken from Kenyon et al. (2005) and Burningham et al. (2005b). Kenyon et al. (2005) obtained spectroscopy of a photometrically selected sample using a ‘close’ selection around the suspected sequence in a CMD, which is potentially photometrically biased. Memberships were then confirmed on the basis of measurements of RV and EWs (equivalent widths) of $Na I$ consistent with the group mean. Burningham et al. (2005b) however, used a ‘broad’ colour–magnitude selection. The memberships were also confirmed here via RV and $Na I$ and $Li I$ EWs. Burningham et al. (2005b) showed that using a ‘broad’ selection does not reveal significantly more members, implying that using members from Kenyon et al. (2005) does not significantly bias our results. Of the members from Kenyon et al. (2005), only those satisfying all the criteria were included. In the case of Burningham et al. (2005b) a selection of >80 per cent probability of membership was applied to ensure a high percentage of genuine group members (Table 21).

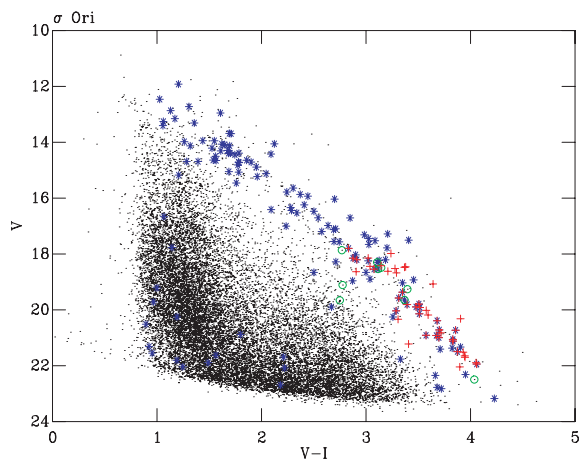


Figure A2. The full catalogue for the σ Ori field (dots). Circles are members from Burningham et al. (2005b), while asterisks are X-ray sources from Sanz-Forcada et al. (2004). Crosses are members from Kenyon et al. (2005).

X-ray positions were taken from Sanz-Forcada et al. (2004). We included those for which Sanz-Forcada et al. (2004) (Table 20) found no optical counterpart and then cross-correlated the positions with our catalogue. The Sanz-Forcada et al. (2004) positions were used in preference to *ROSAT* data due to the higher spatial resolution of *XMM-Newton*. Jeffries et al. (2006) shows that PMS members of this association are separated into two kinematic subgroups by heliocentric radial velocities, having different ages. In this work all but four stars from the sequence members are at a declination of less than $\delta = -2^{\circ} 18' 00''.0$. This area is dominated by members from group 2 as defined in Jeffries et al. (2006). The resulting CMD is displayed as Fig. A2.

A6 Cep OB3b

Spectroscopic members were taken from Pozzo et al. (2003). They used a broad colour–magnitude selection with subsequent spectroscopic measurements of Li I EW, H α and RV. Pozzo et al. (2003) then used the spectroscopic measurements in conjunction with X-ray measurements to compare each star to the group mean and assign memberships (Table 14). H α memberships were taken from Ogura et al. (2002) (Table 17), who used a photometrically unbiased narrow-band imaging survey. The X-ray data were taken from Naylor & Fabian (1999), supplemented with the second *ROSAT* PSPC catalogue. The latter contained two pointings; the one from Naylor & Fabian (1999), and a second, non-overlapping field. Both the unpublished and Naylor & Fabian (1999) catalogues were therefore used (Table 14), but wherever possible we took the positions from the Naylor & Fabian (1999) reduction. In addition the X-ray sources from Getman et al. (2006) have been included (Table 18). These sources are from the *Chandra* ACIS detector, and subsequently have a much higher spatial resolution and sensitivity than *ROSAT*. Both the *ROSAT* and *Chandra* data have been used as the latter is centralized on a smaller FOV about the cluster core, while many of the *ROSAT* detections are outside this area. In the cases where a Getman et al. (2006) source lies within the positional error box of the sources from the *ROSAT* catalogues, the *Chandra* ACIS positions have been used. Periodic variables come from Littlefair et al. (in preparation) (Table 16). The resulting CMD is displayed as Fig. A3.

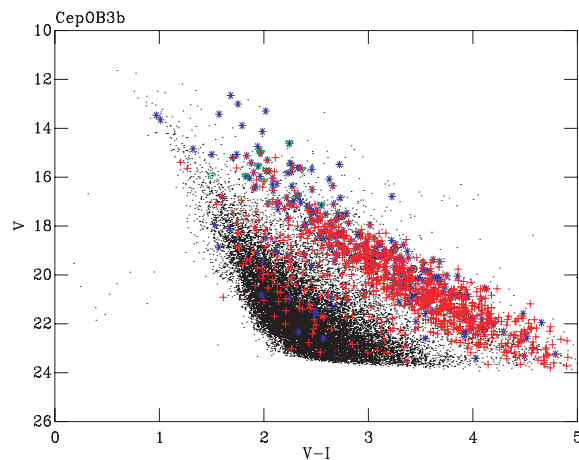


Figure A3. The full catalogue for the Cep OB3b field (dots). Asterisks are X-ray sources from Naylor & Fabian (1999), Getman et al. (2006) and the Second *ROSAT* PSPC catalogue. Triangles are members from Pozzo et al. (2003). Circles are H α sources from Ogura et al. (2002). Crosses are the periodic variables from Littlefair et al. (in preparation).

A7 IC 348

Spectroscopic and H α data were taken from Herbig (1998). He used photometry and a wide-field H α survey (grism spectrograph), discarding H α EWs $< 2 \text{ \AA}$ (Table 27). Follow-up spectroscopy was undertaken on 80 stars within the field. Herbig (1998) classified the spectra by comparison with dwarf spectral standards, using these to derive extinctions (Table 26). The second set of spectroscopic members were taken from Luhman et al. (2003) (supplemented by Luhman (1999), Luhman et al. (2005a), Luhman, McLeod & Goldenson (2005b) and Luhman et al. (2003)) (Table 26). In Luhman et al. (2003) spectral types were assigned using various models and then extinctions calculated by dereddening the stars on to standard colours. The individual extinctions from Herbig (1998) and Luhman et al. (2003) are used here. X-ray members were taken from Preibisch & Zinnecker (2002) (Table 24), where H α and *Chandra* data were presented with extinctions included. Preibisch & Zinnecker (2002) also include extinctions from a range of literature sources. We supplemented the X-ray data from Preibisch & Zinnecker (2002) with a portion of the Second *ROSAT* PSPC catalogue (Table 25). Periodic variables were taken from Cohen et al. (2004) and Littlefair et al. (2005) (Table 23), both being derived from *I*-band wide-field surveys. The sequence with the members is displayed as Fig. A4.

A8 λ Ori

Likely PMS members were selected from an *R*, *R-I* CMD. This sample was then spectroscopically observed using Li EW as an indicator of membership. The have used only those stars showing significant evidence for Li.

A9 NGC 2362

Dahm (2005) used a wide-field H α survey to identify a sample of 200 stars, which lay above the ZAMS in an optical CMD. This sample is then used for follow-up spectroscopy, using H α EW and Li EW as membership criteria. The members so identified are used here.

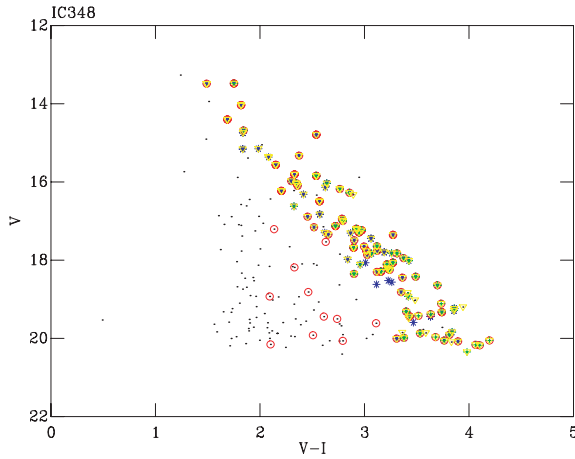


Figure A4. The full catalogue for the IC 348 field (dots). The asterisks are X-ray sources from Preibisch & Zinnecker (2002) and the Second *ROSAT* PSPC catalogue. Circles are the periodic variables from Cohen et al. (2004) and Littlefair et al. (2005). Crosses are $H\alpha$ sources from Herbig (1998). Triangles are spectroscopic members with extinctions from Luhman et al. (2003) and Herbig (1998).

A10 IC 5146

Herbig & Dahm (2002) used a wide-field survey to identify any stars showing $W(H\alpha) > 5 \text{ \AA}$. We used stars with known spectral types and exhibiting a $W(H\alpha) > 5 \text{ \AA}$, discarding any stars lying below the Pleiades MS following Herbig & Dahm (2002).

A11 NGC 6530

X-ray members are from Prisinzano et al. (2005) using the *Chandra* ACIS detector. $H\alpha$ members are taken from Sung et al. (2000).

APPENDIX B: LITERATURE DISTANCES AND EXTINCTIONS

When obtaining parameters from the literature, as far as possible we avoided using values derived from PMS fitting, since we wish to derive ages independent of existing PMS isochrones. However, values derived from MS fitting (i.e. fitting the upper part of the sequence) were used as these are independent of assumptions about the age. The following section details the literature sources used for each field. Tables B1, B2 and B3 provide summaries of the information used.

B1 h and χ Per

Since the catalogues were combined and normalized to χ Per, only the parameters for this cluster were required. The parameters for this cluster were taken from Capilla & Fabregat (2002), $A_V = 1.71$, $d_m = 11.7 \pm 0.1$ mag. This study fitted narrow-band photometry with MS isochrones. The values of extinction and distance modulus are in line with other recent determinations, such as, Marco & Bernabeu (2001) $E(b - y) = 0.39 \pm 0.05$ and $d_m = 11.56 \pm 0.20$; Slesnick et al. (2002) $d_m = 11.85 \pm 0.05$ and $E(B - V) = 0.56 \pm 0.01$.

B2 NGC 2547

Claria (1982) undertook a photoelectric survey in *UBV* and found 22 probable radial velocity members with $(B - V) < 0.1$. Using individual reddenings to MS intrinsic colours he derived $A_V = 0.192$,

from $E(B - V) = 0.06 \pm 0.02$ mag, with $d_m = 8.27$ mag. Robichon et al. (1999) used *HIPPARCOS* parallax data to calculate a $d_m = 8.18^{+0.29}_{-0.26}$ pc. This later distance modulus used an alternative method to isochronal or intrinsic colour fitting, so will be most useful here. The studies used for memberships in Section A2 have all confirmed within uncertainties the parameters found in these two cases. The carried forward values are; $d_m = 8.18^{+0.29}_{-0.26}$ mag and $A_V = 0.192$.

B3 ONC

H_2O MASER measurements are used in Genzel et al. (1981), where expansion velocities of molecular clouds were used to infer the distance modulus. A result of $d_m = 8.38 \pm 0.37$ mag was obtained. This along with extinctions from Hillenbrand (1997) were used for this field.

B4 NGC 2264

In Dahm & Simon (2005) a summary of values from previous studies is presented along with the methods of calculation. All the entries listed are from forms of isochrone fitting, but we consider only those studies fitting the MS. Sung, Bessell & Lee (1997) used colour-magnitude selection in $R - H\alpha$, then fitted the ZAMS to assumed B type stars. An average distance modulus of 9.4 ± 0.25 mag and $A_V = 0.23$ resulted. Perez, The & Westerlund (1987) used shifts of individual OB type stars to intrinsic colours leading to $A_V = 0.19$ and $d_m = 9.88 \pm 0.17$ mag. Park et al. (2000) selected stars using $H\alpha$ and X-ray emission, then used MS isochrone fitting with the bright stars, deriving a distance modulus of 9.4 ± 0.10 mag and $E(B - V) = 0.066 \pm 0.034$. An average of these values has been taken being $d_m = 9.6$ mag and $A_V = 0.21$.

B5 σ Ori

Brown, de Geus & de Zeeuw (1994) found parameters using the lower part of the sequence, without the use of isochrones. Derivations of surface gravity from narrow-band photometry were calibrated to intrinsic colours of the theoretical and empirical models in Straižys & Kuriliene (1981). Brown et al. (1994) used MK spectral types in conjunction with effective temperature and absolute bolometric magnitudes to calculate surface gravities and radii of stars. In Straižys & Kuriliene (1981) however the calibrations were done without taking into account PMS or post MS objects. Brown et al. (1994) applied these calibrations to all spectral types, clearly at the age of around 3 Myr many of these stars are indeed PMS objects. A set of subgroups were selected and the subgroup 1b in this paper covers our field. The values for this subgroup were given as $d_m = 7.8 \pm 0.39$ mag, with a value of $E(B - V) = 0.06$. The distance modulus from *HIPPARCOS* parallax measurements is quoted as $d_m = 7.73^{+0.84}_{-0.60}$ to the star σ Orionis. The large uncertainties make this value unusable. Therefore the values taken forward were from Brown et al. (1994), namely $d_m = 7.8 \pm 0.39$ mag and $E(B - V) = 0.06$ ($A_V = 0.18$).

B6 NGC 7160

Sicilia-Aguilar et al. (2004) and Sicilia-Aguilar et al. (2005) used membership criteria described in Section A4. These papers used spectroscopically derived spectral types and intrinsic colours to calculate the extinctions, and MS isochrone fitting for the distance modulus. The resulting values were $A_V = 1.17$ and $d_m = 9.77$ mag.

B7 Cep OB3b

Moreno-Corral et al. (1993) used optical and IR photometry of O, B and A type stars. These were compared with MS calibrations to calculate individual extinctions and distance moduli, which were then averaged. Pozzo et al. (2003) recalculated these parameters from the Moreno-Corral et al. (1993) individual extinctions and distance moduli, but excluded star 11 from Blaauw, Hiltner & Johnson (1959) which is of dubious membership. The resulting values which we also adopted were $d_m = 9.65 \pm 0.20$ and $A_V = 2.81 \pm 0.10$.

B8 IC 348

We adopted the distance modulus of Strom, Strom & Carrasco (1974), who used *UBVKL* photometry of 20 stars with $V < 14$ believed to be cluster members, in conjunction with various literature spectral types and MK classifications to derive a distance modulus of $7.5^{+0.14}_{-0.16}$ mag. This is the same distance modulus as that derived to the Per OB2 association, $d_m = 7.5$ mag. A full discussion of the distance to IC 348 is presented in Herbig (1998). The extinctions for this field were individual star extinctions and were from Herbig (1998) and Luhman et al. (2003).

B9 λ Ori

We have used the *HIPPARCOS* distance modulus to this cluster, $d_m = 7.90 \pm 0.17$. The extinction to this cluster is calculated in Diplás & Savage (1994) as $E(B - V) = 0.12$, equating to $A_V = 0.36$.

Table B3. Extinctions (mag) from Q-method and from the literature.

Field	Q-method	Literature
χ and h Per	1.571 and 1.728	1.82 and 1.71
NGC 2264	0.371	0.22
NGC 2547	0.15	0.192
Cep OB3b	2.882	2.81 ± 0.1

B10 NGC 2362

Balona & Laney (1996), using narrow-band photometry of B-type stars derive $A_V = 0.31$ and $d_m = 10.87 \pm 0.03$. Moitinho et al. (2001) also used the B-type stars to obtain $A_V = 0.31$ and $d_m = 10.85$. The values adopted here are 10.87 ± 0.03 and $A_V = 0.31$.

B11 IC 5146

Herbig & Dahm (2002) derived a distance modulus from a comparison of the early-type stars with models yielding $d_m \simeq 10.4$. They then calculated the reddening by assuming their distance modulus and using the known spectral types of a selection of 38 stars, to yield $A_V = 3.0 \pm 0.2$. We have adopted $d_m \simeq 10.4$. The individual extinctions used for the B type stars to calculate the distance modulus have been used, with the average extinction being applied to the remaining stars. Due to the need for individual extinctions, as with the ONC and IC 348 the extinctions were applied before fitting.

Table B1. The members for each field are available in this format at http://www.astro.ex.ac.uk/people/timm/Catalogues/table_tables.html. The data are listed as tables 4–29. This table is a sample only, to indicate the format of the online tables.

Field & CCD (field.ccd)	ID	RA	Dec.	x position (CCD)	y position (CCD)	MAG	Uncertainty	FLG	COL	Uncertainty	FLG
1.04	173	02 22 19.173	+57 08 11.19	978.686	2770.194	12.230	0.010	OO	0.386	0.016	OO

Table B2. Extinction, d_m , ages and sources.

Field	A_V	Source	Method	d_m (mag)	Source	Method	Age (Myr)	Source
NGC 2547	0.15	1	Q-method	$8.18^{+0.29}_{-0.26}$	11	<i>HIPPARCOS</i>	30–45	27
χ Per	1.57 ± 0.079	2	Q-method	11.7 ± 0.1	10	MS fitting	12.6	2
NGC 2264	0.371	4	Q-method	9.6	13	Average of many values	3	
NGC 7160	1.17	5	Intrinsic colours	9.77	14	Isochrone fitting	10	5
Cep OB3b	2.882	6	Q-method	9.65 ± 0.20	15	Spectroscopy	5.5	20
σ Ori	0.18	8, 9	Iso fitting	7.8 ± 0.39	17	<i>HIPPARCOS</i>	3	17
ONC	A*	19	Spectral classes	8.38 ± 0.37	18	H ₂ O MASER	≈ 0.8	19
IC 348	A*	7	Spectral classes classification	$7.5^{+0.14}_{-0.16}$	16	<i>HIPPARCOS</i>	2–3	7
λ Ori	0.37	24	Spectral classes	7.90 ± 0.17	24	<i>HIPPARCOS</i>	4, 6–7	28
NGC 2362	0.31	25	Average of literature values	10.87 ± 0.03	26	MS fitting	$\simeq 1.8, 3.5$ –5	25
IC 5146	3.0 ± 0.2	23	Spectral type classification	10.4	23	MS fitting	1	23
NGC 6530	1.09	22	MS fitting	10.48	22	MS fitting	2.3, 1.5 or 0.5–1.5	29, 30 and 31

A*: Individual values from sources indicated.

(1) Claria (1982), (2) Slesnick et al. (2002), (3) Sanner et al. (2000), (4) Mendoza & Gomez (1980), (5) Sicilia-Aguilar et al. (2004), (6) Jordi et al. (1996), (7) Herbig (1998) and Luhman et al. (2003), (8) Béjar, Zapatero Osorio & Rebolo (1999), (9) Sherry, Walter & Wolk (2004), Brown et al. (1994), (10) Capilla & Fabregat (2002), (11) Robichon et al. (1999), (12) Sanner et al. (2000), (13) Dahm & Simon (2005), (14) Sicilia-Aguilar et al. (2004), (15) Pozzo et al. (2003), (16) Herbig (1998), (17) Sherry et al. (2004), (18) Genzel et al. (1981), (19) Hillenbrand (1997), (20) Jordi et al. (1996), (21) Diplás & Savage (1994), (22) Prisinzano et al. (2005), (23) Herbig & Dahm (2002), (24) Diplás & Savage (1994), (25) Dahm (2005), (26) Balona & Laney (1996), (27) Jeffries & Oliveira (2005), (28) Murdin & Penston (1977) and Dolan & Mathieu (2001), (29) Siess et al. (2000), (30) Sung et al. (2000) and (31) Damiani et al. (2004). The used values of extinction for the lower age sequences is largely inconsequential as the isochrones are parallel to the dereddening vector at the lower mass end.

B12 NGC 6530

Prisinzano et al. (2005) used MS fitting of the stars in the blue envelope. These are MS stars assumed to be at the cluster distance or closer. They calculate $d_m \simeq 10.48$ and use the value of the extinction from Sung et al. (2000). Sung et al. (2000) fitted a ZAMS relation individually to 30 early-type stars, yielding two different average distance moduli, assuming one was due to binarity they adopted the larger distance modulus, $d_m = 11.25 \pm 0.1$ mag. The Q-method is

then used for these early-type stars yielding $A_V \simeq 1.09$. In Prisinzano et al. (2005) a useful summary table of the distance moduli calculated to this cluster is presented along with a summary of the literature of the field. For this study we have used both $d_m \simeq 10.48, 11.25$ and used $A_V \simeq 1.09$.

This paper has been typeset from a \TeX/L\TeX file prepared by the author.